Laboratory simulation of lifted temperature minimum

A thesis
submitted for the degree of
MASTER OF SCIENCE (ENGINEERING)

by

PUNIT TIWARI

ENGINEERING MECHANICS UNIT
JAWAHARLAL NEHRU CENTRE FOR ADVANCED
SCIENTIFIC RESEARCH
BANGALORE - 560 064

MAY 2006

Dedicated To My Parents

DECLARATION

I hereby declare that the work embodied in the thesis entitled "**Laboratory simulation of lifted temperature minimum**" is the result of investigations carried out by me at the Engineering Mechanics Unit, Jawaharlal Nehru Centre for Advanced Scientific Research, Bangalore, India under the supervision of Dr. K.R. Sreenivas and that it has not been submitted elsewhere for the award of any degree or diploma.

In keeping with the general practice in reporting scientific observations, due acknowledgement has been made whenever the work described is based on the findings of other investigators.

Punit Tiwari

CERTIFICATE

I hereby certify that the work embodied in this thesis entitled "**Laboratory simulation of lifted temperature minimum**" has been carried out by Mr. Punit Tiwari at the Engineering Mechanics Unit, Jawaharlal Nehru Centre for Advanced Scientific Research, Bangalore, India under my supervision and that it has not been submitted elsewhere for the award of any degree or diploma.

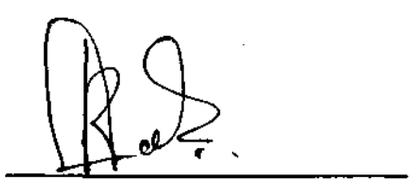

Dr. K.R. Sreenivas
(Research Supervisor)

CONTENTS

Acknowledgements

I would like to sincerely thank Dr. K.R.Sreenivas for his guidance and unstinted support throughout my work.

I also would like to thank Prof.R.Narasimha for his constant inputs and valuable suggestions towards my work.

I am equally grateful to Dr.Vasudeva Murthy, Prof.J.Srinivasan and Prof.Rama Govindarajan for helpful discussions regarding my work.

My sincere thanks to my lab mate Mukund for helping at various stages of the experiments.Thanks are also due to Shreyas, Manikandan, Vinod, Sameen, Faraz, Kaushik, Pinaki, Kirti, Ashish, Saji Varghese and Anjana.

Thanks are also due to Mr.Krishnoji Rao of Microtech Engg for the fabrication of my experimental set up.

I would like to thank Dr.Ranga Uday Kumar of MBGU for giving me permission to use the ice machine. My sincere thanks to Mr.Arokianathan at the workshop for helping me with the fabrication of various parts in my set up.

I would like to thank my friends Archana, Shailesh, Sharmila, Satish, Prashanth, Patrick, Roopesh and Hari Kishore for making my stay in JNCASR memorable.

I am grateful to JNCASR for giving me the opportunity to work at this wonderful place for my M.S. and for providing me with excellent lab facilities to carry out my project.

I would like to acknowledge my parents and brother for their constant support and encouragement.

Last but not the least, I am grateful to The Almighty for providing me with patience and perseverance to pursue my M.S. degree.

List of figures

1. Introduction

1.1 The lifted temperature minimum

The lifted temperature minimum phenomenon or the Ramdas Paradox has been a longstanding micrometeorological puzzle. It concerns the vertical distribution of air temperature. During the day time, the mean temperature on the ground remains higher than the air temperature which decreases sharply in the thermal boundary layer; then mean temperature changes a little in the mixed layers above it and finally temperature follows the adiabatic lapse rate, Γ (curve 1 in Figure 1.1). Normally, after the sunset, ground loses heat faster than the air due to its high emissivity, thus the minimum temperature occurs at the ground followed by a raise in the temperature as indicated by curve 2 in Figure 1.1 (normal radiative type). However, Ramdas and Atmanathan [1932] reported that on calm and clear nights in Pune and other places in India, they observed the minimum temperature not at the ground but at a height of few decimeters above it as indicated by curve 3 in Figure1.1. These observations caused considerable surprise for several reasons. It went counter to the then existing view that following sunset a temperature inversion always develops at ground. This view has apparent support from normal observations of air temperature (Sutton 1953), but it must be remembered that such observations usually stop at the standard screen height of 4 ft (1.22 m). Below this height, rapid ground cooling after sunset was expected by radiative heat transfer, thus minimum temperature should occur at the ground surface. There is no obvious reason why air temperature should fall below the ground temperature. Whereas, ground is a good radiator compared to air, hence it was believed to cool to a temperature below that of air above it. Moreover, a temperature minimum above ground should lead to Rayleigh-Benard instability, so it is not clear how it can be sustained for several hours (virtually till sunrise, as Ramdas [1932] reported), even assuming that it had risen as some transient.

Ramdas and Atmanathan found that the layer of air at few decimeters above the ground remain cooler than that at the ground for well over three hours. Although these results were at first treated with skepticism, they have been confirmed by many other investigators in different parts of the world, leading to what has since become known as the lifted minimum phenomenon or Ramdas Paradox (R.Narsimha [1991]).

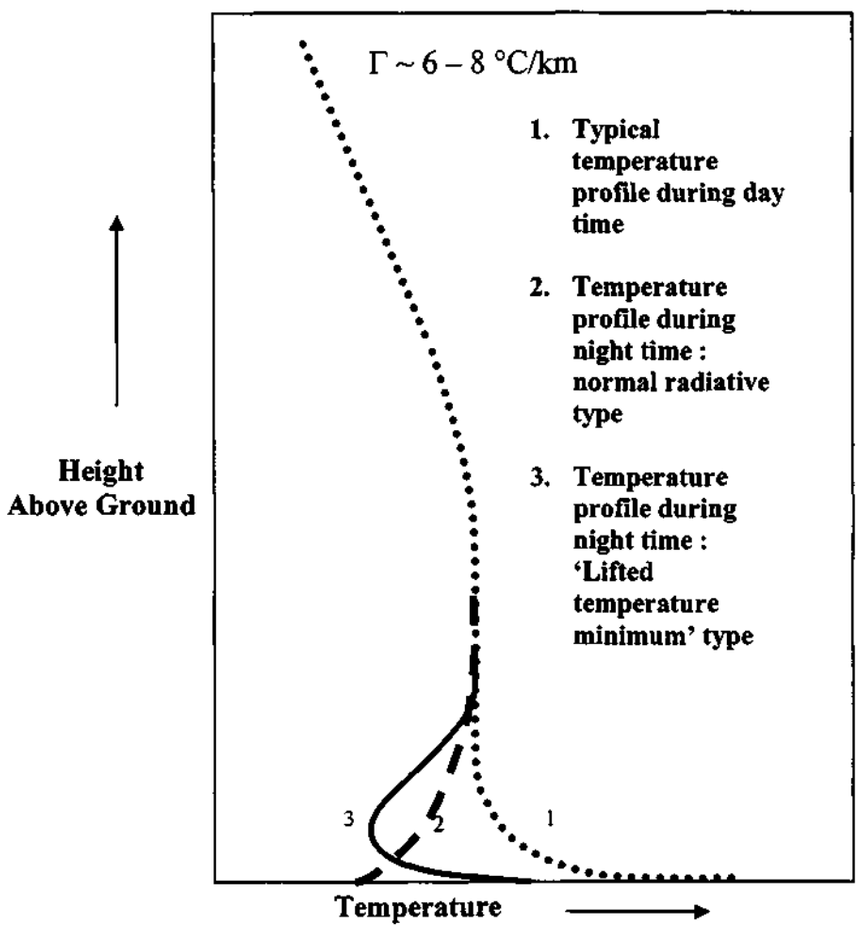

Figure 1.1. Typical vertical temperature profiles observed close to the ground.

The weather and climate near the ground, in particular the vertical distribution of air temperature, are important factors in agricultural meteorology and horticulture applications. It affects the formation of fog and dew, dispersion of pollutants and the occurrence of frost; Lake (1956) quotes studies showing how tomato plants spread out on bare soil start freezing from the top. The phenomenon should also be important for retrieval of correct surface temperatures from remotely sensed radiation data from satellites.

In order to understand the nature of the observed temperature profiles, a clear appreciation of the relevant importance of the various heat transfer processes near the ground is necessary. The major processes involved are advection, convection and radiation. Advection plays a major role only when there are strong horizontal

temperature gradients and can be neglected if the fetch (The distance upstream of a measurement site, receptor site, or region of meteorological interest, that is relatively uniform) to height ratio is large (Oke [1970]).

1.2 Literature Survey

Ramanathan and Ramdas [1935] calculated the cooling of air (assumed to be at 300 K) near the ground as a result of radiative exchange with the upper atmosphere, and found it to be 0.11 K/h if the upper atmosphere was assumed to be at a mean temperature of 270K (and higher if the upper atmosphere was cooler). They then concluded that the air near the ground cools not only by eddy diffusion and radiation exchange with the ground but also by radiation exchange with the upper atmosphere. According to them the coolest air layer does not settle down to the ground because the effects of viscosity and heat conduction keep the thin ground layer in stable equilibrium.

Lake [1955], who apart from making his own careful observations also analyzed several others, concluded that the air on clear night must lose heat by some mechanism other then convection and conduction to the surface. To quote him, "It has been already suggested that radiation exchange may provide a mechanism for such a loss. In this case the air would continue to lose heat by radiation until it reached radiative equilibrium with its surroundings, and this process might be retarded or assisted by other heat transfer processes such as conduction and eddy diffusion. As the duration of stable conditions increased, the layer in which the maximum rate of cooling took place became further and further away from the surface, indicating that the lower layers were approaching thermal equilibrium with their surroundings".

Raschke [1957] based on his interesting observations in Pune, points out that during nights when the wind is generally strong and normal radiation type of distribution is the rule, a lifted minimum phenomenon can occur whenever the wind speed drops below a critical value (of the order of 0.5 m/s). Also the lifted minimum can be broken down by just waving (for example) a wooden lath. These observations show that very little turbulent transport is required to suppress the formation of lifted minimum.

Geiger [1965] referring to earlier results, concludes that the lifted minimum phenomenon is caused by long-wavelength radiation; if mixing is particularly low,

which is usually the case at nights close to the ground surfaces, the influence of radiation predominates and the minimum is found about 10 cm above the ground. Further, estimating the diffusion coefficient based on the calculations of Moller [1955] and the others, Geiger suggests that there is a gradual change from eddy diffusion at a height of 1 to 2 m to molecular diffusion of heat in the vicinity of the surface.

Moller has suggested (cf. Zdunkowski [1966]) that if a haze layer of water droplets existed on the ground a lifted minimum could be produced due to strong radiative cooling. Zdunkowski [1966], pursuing the above suggestion, proposed a set of time-dependent partial differential equation to describe radiative and eddy heat transfer and subjected it to an extensive numerical study. He concluded that the cold layer is due to the combined effects of turbulence and radiative flux divergence. Zdunkowski's numerical experiments reveled that in the absence of turbulence in the specified layer, a near isothermal layer was created instead of a lifted minimum. However a combination of strong radiative cooling and very weak turbulent mixing (for which he had to assume values of the diffusivity less than the molecular value, which is clearly unphysical) does produce a lifted minimum, but even a slight amount of turbulent mixing tends to create isothermal temperature profile.

Coantic and Seguin [1971] made an analytical numerical study of the interaction between turbulent and radiative transfer in the surface layer of the ocean. Assuming steady state and horizontal homogeneity in the atmospheric boundary layer, they derived an expression, which stated that the sum of turbulent and radiative fluxes in the surface layer was independent of height. This expression was then used to study the variation of turbulent fluxes as a result of variation in the radiative fluxes. They computed the radiative flux divergence based on a logarithmic distribution of temperature near the surface for various values of surface layer parameters. Their computations always showed a maximum in the radiative flux divergence profiles at a height of order 10 cm above the surface so long as the temperature profile was monotonically increasing with height. They then suggested that this maximum in radiative flux divergence could be responsible for the lifted minimum.

Kondratyev [1972], analyzing Oke's observations, wrote: "It can be considered that the raised temperature minimum is a phenomenon of non-turbulent nature. Apparently, this regime of the near surface air layer, which is also characterized be abnormal temperature and humidity profiles, is determined by the

mechanism of the radiative heat exchange. The fact that vertical temperature gradients are in this case accompanied by very low gradients of wind velocity and humidity is another argument in support of this opinion. It is possible; however, that turbulent mixing contributes as well".

Paltridge and Platt [1976] explain the formation of fog near the ground by referring to the work of Fleagle and Businger, in which the radiative flux divergence was computed from an observed temperature profile over a water surface. Based on the maximum found in flux divergence profiles at 10-20 cm level, Paltridge and Platt conclude that "Occurrence of the raised temperature minimum and the initial formation of fog away from the surface is quite common and is essentially a radiative phenomenon". This is exactly similar to the conclusion of Coantic and Seguin [1971].

On the other hand Lettau [1979], based on observations in Antarctica, claimed that the lifted minimum phenomenon is mainly due to turbulent convection near the ground and not due to radiative cooling because the physical conditions (perfectly dry and very cold atmosphere) in Antarctica made longwave radiative fluxes and divergence too small to be of significance.

Thus we find that the majority of the investigators although believe that the radiation to be a dominant factor for the lifted minimum, there is no complete agreement, and the precise mechanism is not clear to say the least. As Scorer (Lake [1956 B]) points out during discussion of the paper by Lake [1956 A], "It is easy to understand that if cold air is above warmer ground there will be a 'viscosphere' in which molecular conduction is paramount. Above this, either radiation or convection will be dominant, and in this case it appears to be radiation, but it is difficult to see how a temperature minimum so close to, but away from the surface is produced by radiation. I remain puzzled – could the radiation experts tell us what they can and can not explain with realistic models".

Attempts have been made with some models but the confusion remains. For example the computations of Coantic and Seguin [1971] and Paltridge and Platt [1976] assume a monotonic temperature profile, so it is not clear that a maximum in the radiative flux divergence will remain when there is a non-monotonic profile characteristic of a lifted minimum. On the other hand, Zdunkowski [1966] requires a haze layer near the ground to simulate a lifted minimum in his model even though none of the observations indicate a haze layer. Further the roles of convection and molecular diffusion are not clear; as Lake [1956] remarks," Moller [1955] insists that

in all the cases he investigated radiative processes were swamped by convective process, but Falckenberg, whose theory of 'radiative pseudo-conduction' is well discussed by Geiger in his book on The climate near the ground, maintained that the reverse was often true. Thus the difficulty seems to lie in assessing quantitatively the part played by convection and molecular diffusion".

Many of the studies seem to indicate that radiative heat transfer is the cause for the formation of "Ramdas layer". All of them, however, either assumed unrealistically low value for the thermal conductivity of air or alluded for the presence of haze layer (which is not observed in most of the experiments) to explain this phenomenon Vasudev Murthy *et al* (1993), for the first time, presented a model (VSN model) based on radiative heat transfer to successfully explain the formation of Ramdas layer without the need to assume unrealistic value for the thermal conductivity of air or allude to the presence of haze layer. They solved unsteady, one-dimensional heat equation with molecular, convective and radiation heat transfer components. Radiative heat transfer in the air, with the participating gas like water vapor was modeled by assuming it to be a gray gas whose emissivity/absorptivity is a function of water vapor path length as suggested by Zdunkowski [1965].

Results from the VSN model give physical explanation for the lifted minimum. They showed that the lifted minimum occurs due to the interaction of molecular diffusivity and radiative heat transfer. In the small water vapor path length limit (close to the ground), the emissivity (absorptivity) of air-water vapor mixture raises sharply with the water vapor path length (or with Z, where Z is the height above the ground). This steep increase in emissivity near the ground, coupled with ground emissivity not equal to one, leads to a large divergence in the net radiative heat flux near the ground. The absolute value of this divergence has a maximum value at the ground and sharply reduces to zero value within a meter height. Thus one could get strong cooling on the ground, however, due to molecular conductivity of air and the large heat capacity of the ground, minimum shifts to few decimeters above the ground.

Ragothaman *et al* [1999] extended the work of VSN [1993] to investigate the time evolution of near-ground temperature distributions through numerical simulations. They demonstrated that, if the surface emissivity is not too close to unity, a lifted minimum can appear shortly after sunset, but its subsequent evolution, depending strongly on ground cooling rate, can lead to (i) monotonic growth, (ii) near

steady-state, or (iii) growth followed by collapse. Solutions of the model to an appropriately formulated " turbulent transport episode" reveal that the lifted minimum disappears after the commencement and reappears after the cessation of the gust in times of order 10-20 seconds, in qualitative agreement with the observations of Raschke [1957]. However, full recovery to the no-gust state takes times of order 10^3 seconds after the episode. This behavior was identified with a two-time response of the cold layer, involving a quick radiative adjustment followed by a slow diffusive relaxation.

Saji Varghese *et al* [2003] used a band model for the simulation LTM and were capable of simulating the LTM. They replaced the Broad band flux emissivity scheme in VSN [1993] by a Band model for longwave radiative transfer calculations. The intensity and height of the predicted LTM were lower than the values typical of observations. This was thought to be due to the extremely small temperature slip produced by their analysis, confined to atmosphere only. Significantly, the cooling rates were several times lower than values given by the flux emissivity model VSN [1993]. Effect of ground emissivity on temperature profiles was observed up to heights of almost 1 km. Most importantly they got radiative cooling for the case when ground emissivity was taken as 1 (black) which was not there in VSN [1993].

The thrust of the present work is to try and reproduce the phenomenon in the lab. As we know that, the temperature minimum above ground should lead to Rayleigh-Benard instability. Hence, it would be interesting to survey previous works relating to temperature profile and stability in a radiatively participating medium. The effect of radiation on the other modes of heat transfer is of interest because of its importance in the fundamental understanding of heat transfer in natural convection and in practical applications. These applications include systems such as solar collectors, furnaces, heat exchangers and many energy storage devices; manufacturing processes such as crystal growth and processing of silicon wafers; and natural phenomenon such as the spread of fire.

Goody [1956] applied linear stability theory to determine critical Rayleigh number for the limiting cases of optically thin and thick media bounded by free surfaces. Following Goody, Spiegel [1960] treated the same problem with a wide range of optical thickness and for black rigid bounding surfaces. Lan and Ezekoye [2003] showed by their stability analysis that, the effect of radiative transfer on Rayleigh-Benard convection is to stabilize the flow field and by increasing the optical

thickness, increases the stability of the fluid to perturbations. Experimental studies of the radiative effects on Rayleigh-Benard convection have also been examined. Gille and Goody [1964] conducted the first experimental study of the effect of radiative transfer on the onset of Rayleigh-Benard convection by comparing data for dry air and NH_3 between parallel aluminum plates maintained at different temperatures. Their experiment indicated that the critical Rayleigh number in NH_3 is greatly increased over the best value for dry air (Ra_c =1786); the maximum observed being Ra_c = 4870. Hence works of different researchers seem to indicate that overall effect of radiative transfer is to stabilize the flow field.

1.3 Objective of present work

Even though VSN model explains the phenomena in a satisfactory manner but still some discrepancies exit. Saji [2003] showed that radiative cooling was present for the case when ground was black, Lettau [1979] observed the phenomena at Antarctica, where radiative cooling due to water vapor was not present. Typical Rayleigh number for the unstable Ramdas layer is of the order of 10^5, but none of the experimental studies shows critical Rayleigh number for the Rayleigh-Benard kind of instability greater than a few thousand. Hence, objectives of the present work are,

1. To explore the possibility of reproducing LTM in the lab.
2. To study the dependence of intensity of the minimum on various parameters.
3. To quantify the effect of radiatively participating medium on temperature profiles.
4. To compare the parametric dependence of the phenomena with theoretical models.

Chapter 2 Numerical Simulations:

In this chapter, details of the numerical procedure are presented. This chapter is divided into four sections. In section 2.1, the governing equations are presented in the context of a combined conduction–radiation problem in one-dimensional plane parallel geometry and are based on the model suggested by Vasudevmurthy, Roddam Narsimha and J. Srinivasan [1993] (hereafter VSN model). The model consists of the energy equation, the equations for radiative transport (modeled by the flux emissivity scheme), and the relevant boundary conditions. In section 2.2, the numerical procedure used to solve the equations is described. In section 2.3, results of the simulations are presented and validated with the results from VSN. Similar calculations were then done for the lab scale model to see the feasibility of reproducing the lifted temperature minimum under lab conditions and to decide the values of the parameters to be used in building the model. In section 2.4, details of these numerical simulations are presented.

2.1 The VSN model:

We consider only calm and clear nights with no advective transport. The air temperature T is approximated as homogenous in the horizontal plane, so that it is a function only of time and the vertical coordinate z. Hence, the problem is completely governed by the one-dimensional energy equation, which may be written as

$$\rho_a C_p \frac{\partial T}{\partial t} = -\frac{\partial Q}{\partial z} \tag{2.1}$$

where ρ_a is the density of air, C_p is the specific heat at constant pressure and Q is the total energy flux, conveniently split into two components Q_m and F, representing, the contributions of molecular conduction (Q_m) and infra red radiation F respectively. The molecular conduction term is simply given by

$$Q_m = -k_m \partial T / \partial z \tag{2.2}$$

where k_m is the thermal conductivity of air.

Equation (2.1) can be written as

$$\frac{\partial T}{\partial t} = K_m \frac{\partial^2 T}{\partial z^2} - \frac{q}{C_p}\frac{\partial F}{\partial u} \tag{2.3}$$

where K_m denotes the molecular thermal diffusivity and $q = \rho_w / \rho_a$ the water vapour mixing ratio. The radiative flux F is most conveniently estimated by flux emissivity method (see Liou [1980] & VSN [1993]; it is assumed that water vapour is the chief atmospheric constituent that is responsible for the radiative flux gradient). Assuming the water vapour density ρ_w known as function of height, we can calculate the flux F at a given height z or the equivalent optical path length u measured from the ground,

$$u(z) = \int_0^z \rho_w(z')dz' \tag{2.4}$$

By our assumption of horizontal homogeneity we consider radiative transfer only in the vertical direction. The net longwave radiative flux F can then be written as

$$F = F_{eg}^{\uparrow} + F_{rg}^{\uparrow} + F_a^{\uparrow} - F_a^{\downarrow} \tag{2.5}$$

where $F_{eg}^{\uparrow}$ is the flux emitted directly by the ground that is received at u (with allowance for the loss by absorption in the intermediate layers, through the factor *1-E(u)*). $F_{rg}^{\uparrow}$ is similarly that part of the down flux incident on the ground, namely $F_a^{\downarrow}(0)$, that is reflected from ground and received at u. $F_a^{\uparrow}$ is the contribution due to the air layers below u and $F_a^{\downarrow}$ that due to air layers above. Figure (2.1) provides a schematic illustration of each of these terms.

$$\begin{aligned}
F_a^{\uparrow} &= \int_0^u \sigma T^4(u',t)\,\dot{E}(u-u')du' \\
F_a^{\downarrow} &= \int_u^{u_\infty} \sigma T^4(u',t)\,\dot{E}(u'-u)du' \\
F_{eg}^{\uparrow} &= \varepsilon_g(1-E(u))\sigma T_g^4 \\
F_{rg}^{\uparrow} &= (1-\varepsilon_g)(1-E(u))F_a^{\downarrow}(0)
\end{aligned} \tag{2.6}$$

where $u_\infty = u(\infty)$ is the total atmospheric path length, ε_g is the emissivity of the ground, $T_g(t)$ is the ground temperature. $E(u)$ is the broad band flux emissivity function

of water vapour. VSN used the function E*(u)* according to a proposal by Zdunkowski and Johnson (1965).

$$\begin{aligned} E(u) &= 0.04902 \ln(1+1263.5\,u) && \text{for } u \le 10^{-2} \\ &= 0.05624 \ln(1+875u) && \text{for } u > 10^{-2} \end{aligned} \tag{2.7}$$

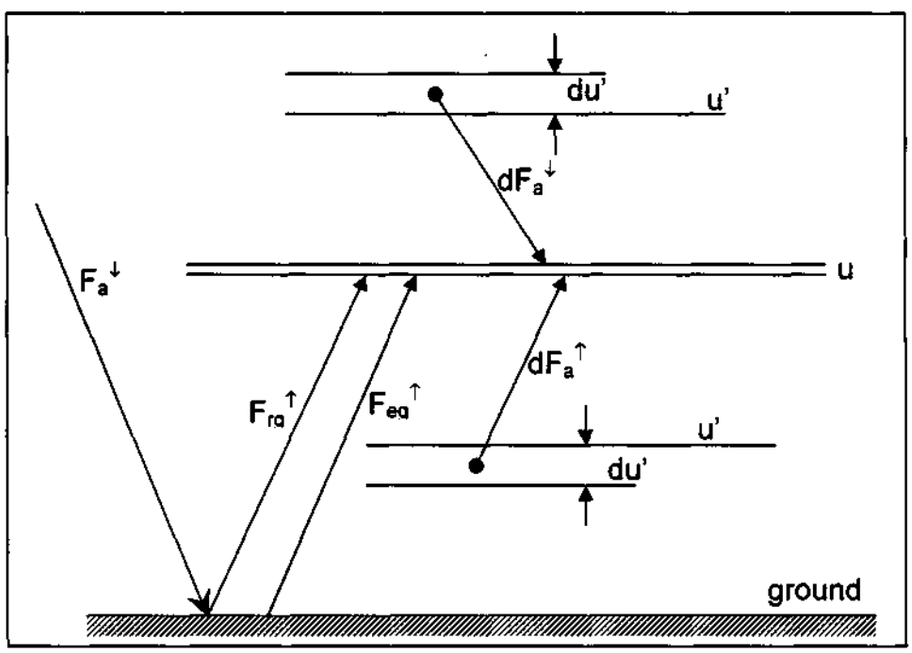

Figure 2.1. Schematic diagram to illustrate different terms contributing to the radiative flux at any given optical depth *u* above ground (R.Narasimha and A.S.Vasudevmurthy [1995].

The energy equations should be supplemented with initial and boundary conditions. Following VSN we will take these as

$$\begin{aligned} &T(z,0) = T_{g0} - \Gamma z \\ &T(0,t) = T_g(t) = T_{g0} - \beta\sqrt{t} \\ &\frac{\partial T}{\partial z}(\infty,t) = -\Gamma \end{aligned} \tag{2.8}$$

Where Γ is specified lapse rate, T_g (t) is the temperature at ground (z=0) at any time t, and $T_g(0)$ is it's value at a suitably defined initial instant t=0. This initial instant corresponds approximately to the time of sunset, and is best determined along with β, where β is a specified ground cooling rate parameter. The basic idea in this approach is to assume a uniform lapse rate Γ in the free atmosphere and discuss the evolution of a thin thermal layer near the ground associated with falling ground temperature.

2.2 Numerical procedure

Equation (2.3) is the overall energy equation (EE) and (2.6) is radiative transfer equation (RTE). For the present case we have participating medium hence, EE and RTE are coupled. The gradient of the radiative flux appears as a "source" term in EE, while the temperature at any point, which is obtained by solving the EE, influences the local radiative fluxes, thereby affecting the solution of RTE. Hence, the two equations are solved sequentially within a larger global loop. First using the initial temperature distribution RTE is solved. The divergence of radiative heat flux, which is calculated from the solution of RTE, is then substituted into the EE, which is next solved to obtain a new temperature distribution. The procedure is then repeated to calculate the temperature distribution at any required time.

The EE and RTE are coupled nonlinear second order partial differential equations; they necessitate solution by numerical means. Equations are solved by finite difference method. For discretization of the EE, Crank-Nicholson method is used, which is an implicit method and unconditionally stable. All the computations were done using MATLAB. To compute the fluxes from equation (2.6), integrations were done by QUAD8 subroutine available in MATLAB. QUAD8 numerically evaluates integral, using an adaptive recursive Newton-Cotes 8 panel rule.

2.3 Validation of the code with VSN results

In this section the energy budget and temperature profiles are presented for each of following cases and compared with the results of VSN. This is done in order to validate the code and methodology for all the numerical simulations hereafter.

Case (1): $\beta = 2$ K/$\sqrt{h}$, $\varepsilon_g = 0.8$, $q = 0.005$;

Case (2): $\varepsilon_g = 1$, rest same as case (1);

Case (3): $\beta = 15$ K/$\sqrt{h}$, rest same as case (1);

Figures 2.2, 2.5 and 2.8 show the energy budget from our simulation for Case1, Case2 and Case 3 respectively. For comparison Figures 2.3, 2.6 and 2.9 show the energy budget calculated by R.Narsimha and A.S.Vasudevmurthy [1995] for the same three cases. A comparison of theses shows good agreement. Case1, which shows a pronounced lifted temperature minimum, provides a baseline case. In Case 2 and Case 3 a single parameter is varied sufficiently from the baseline case to cause the disappearance of the minimum. Figure 2.4, 2.7 and 2.10 show the temperature profile for the three cases. For the case1 we see a pronounce minimum, while for Case2 and Case3 minimum has disappeared.

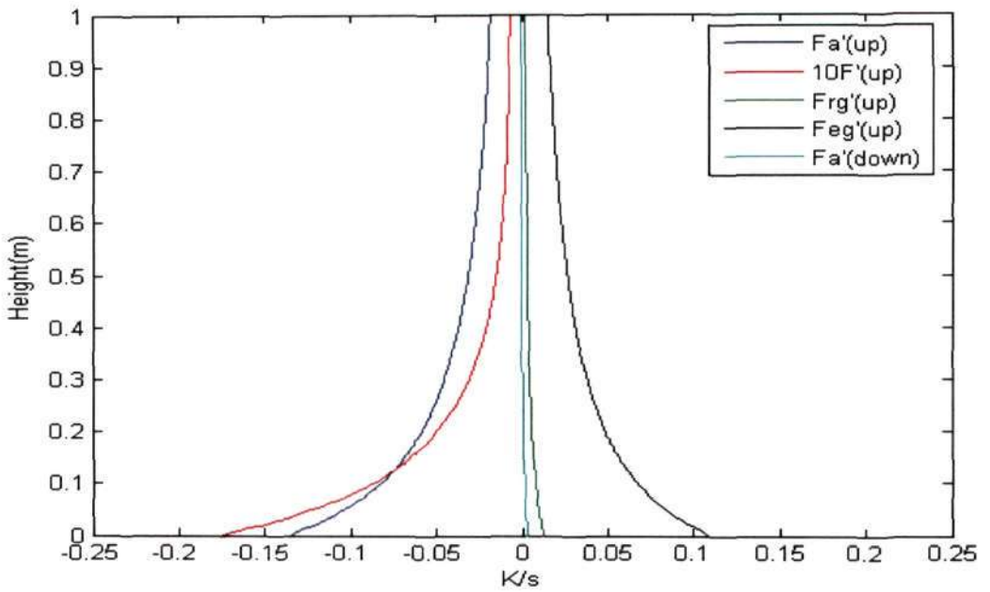

Figure 2.2. Different terms contributing to the energy budget near ground, as a function of height for case I.

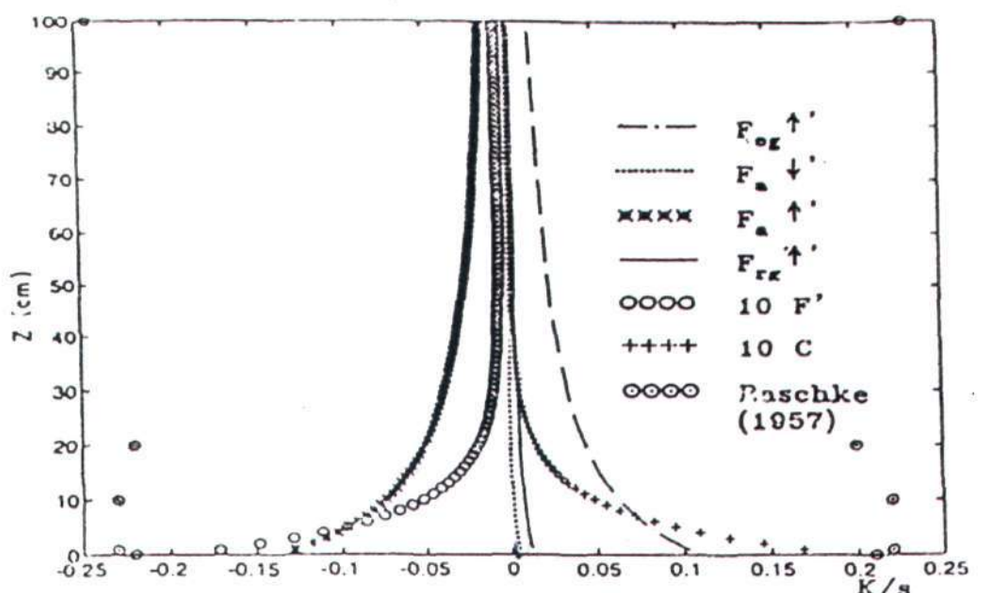

Figure 2.3. Different terms contributing to the energy budget near ground, as a function of height for case I (R.Narsimha and A.S.Vasudevmurthy [1995]).

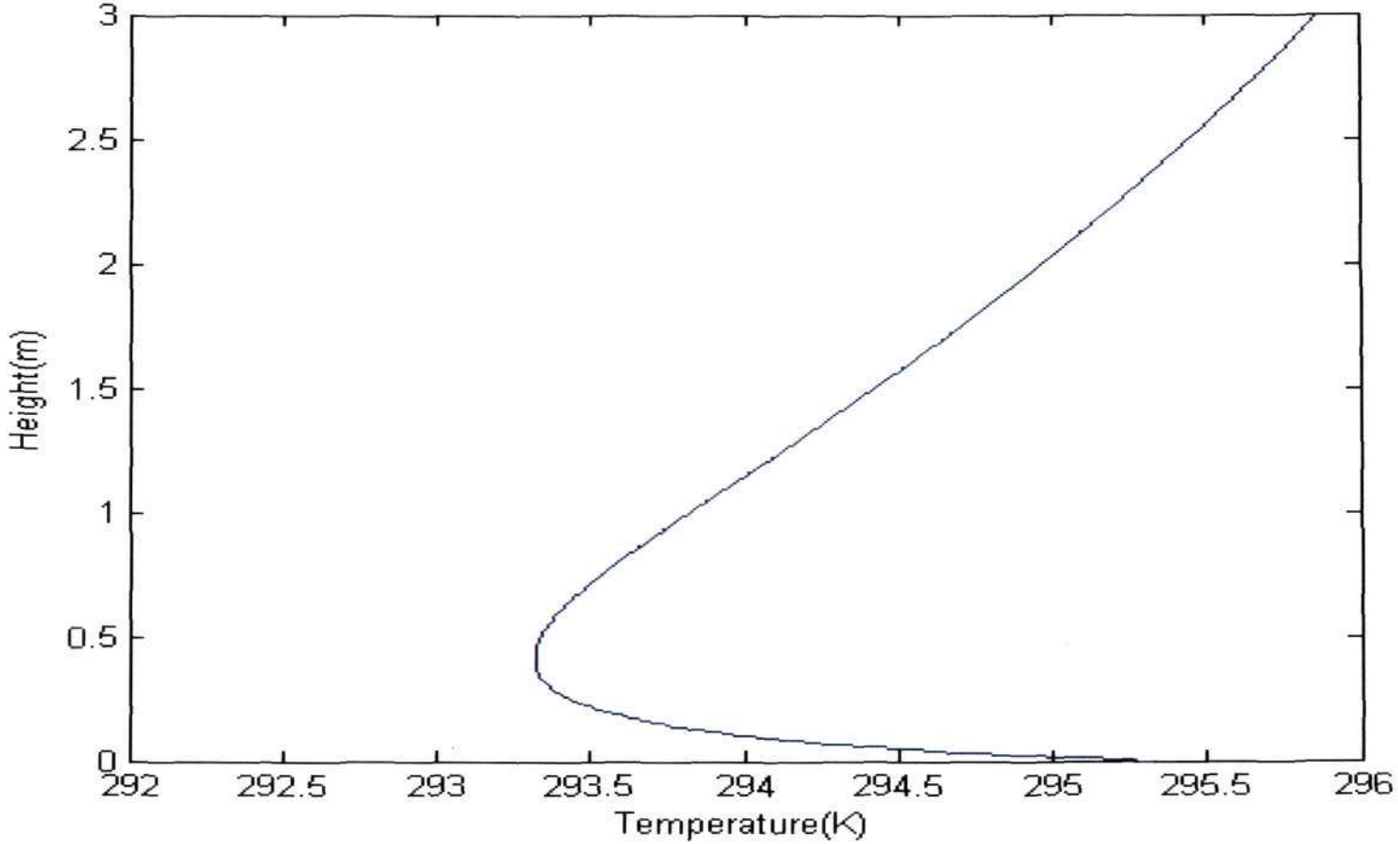

Figure 2.4. Temperature profile for case I.

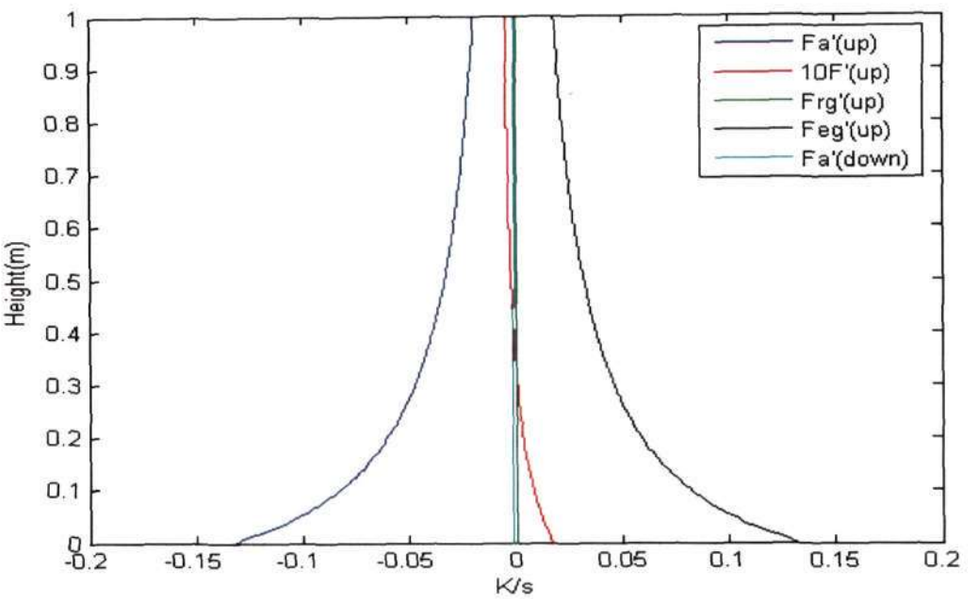

Figure 2.5. Different terms contributing to the energy budget near ground, as a function of height for case II.

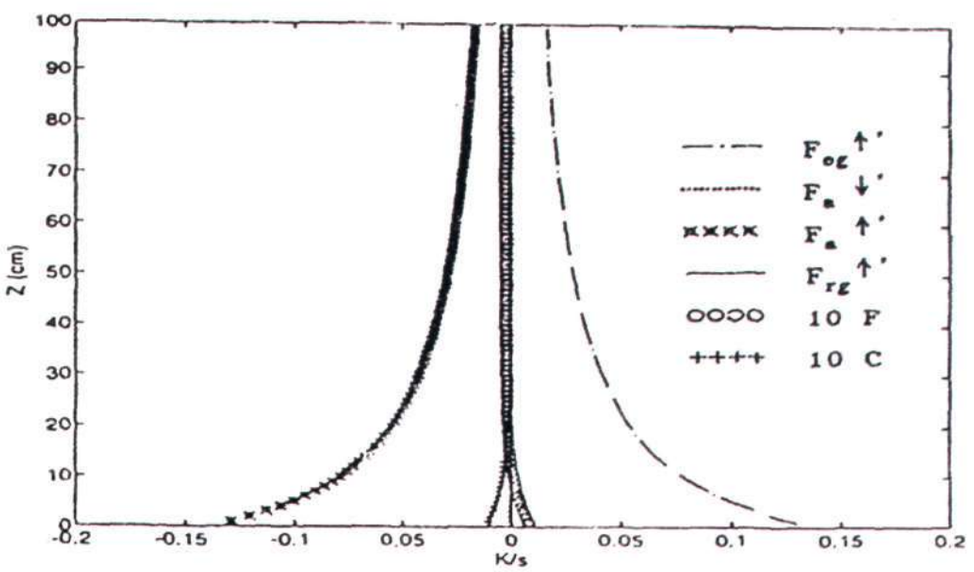

Figure 2.6. Different terms contributing to the energy budget near ground, as a function of height for case II (R.Narsimha and A.S.Vasudevmurthy [1995]).

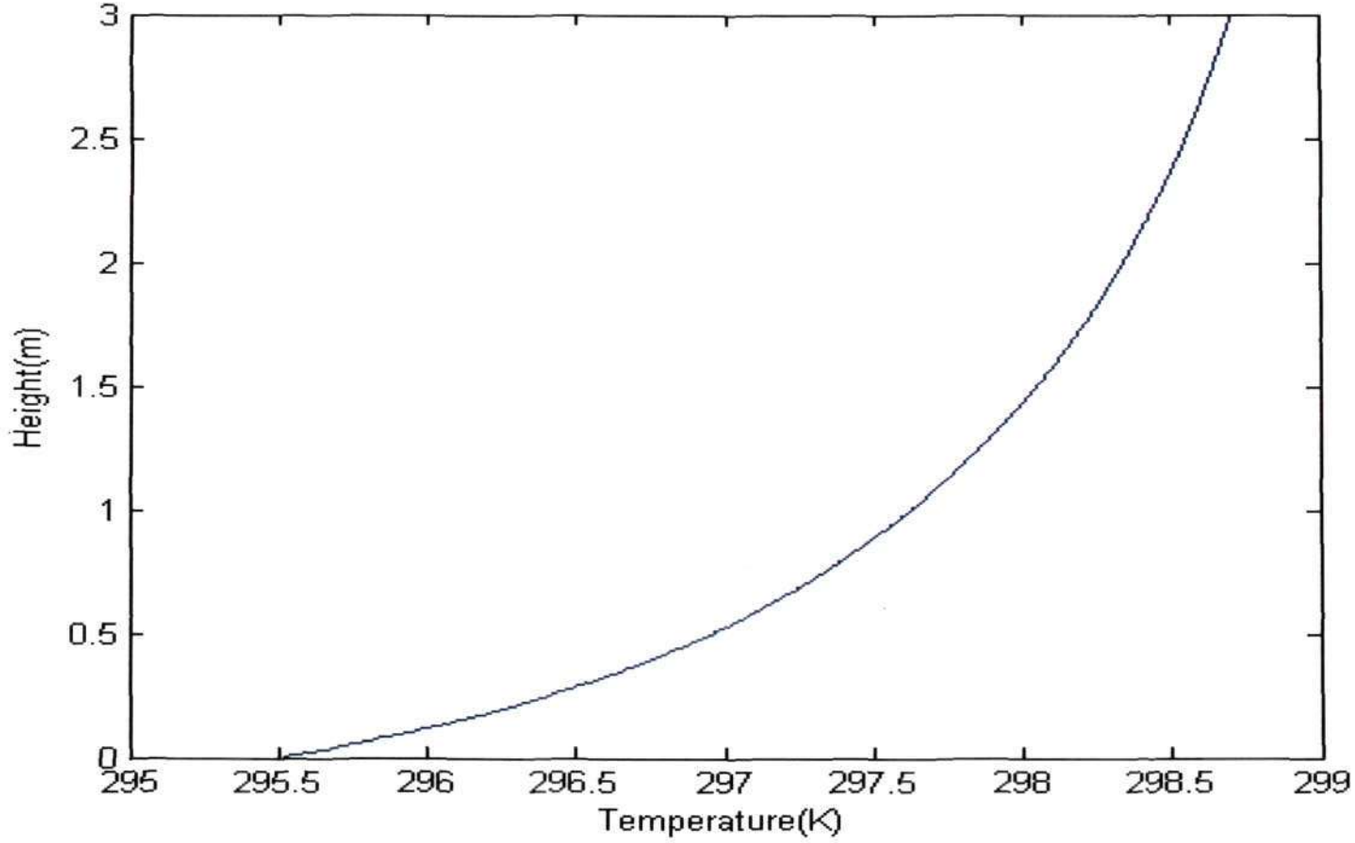

Figure 2.7. Temperature profile for case II.

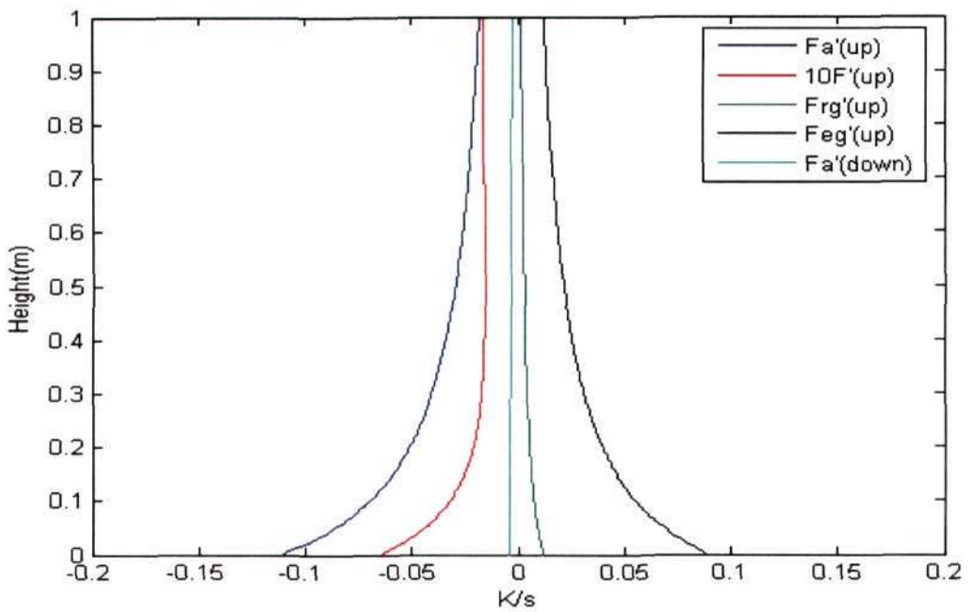

Figure 2.8. Different terms contributing to the energy budget near ground, as a function of height for case III.

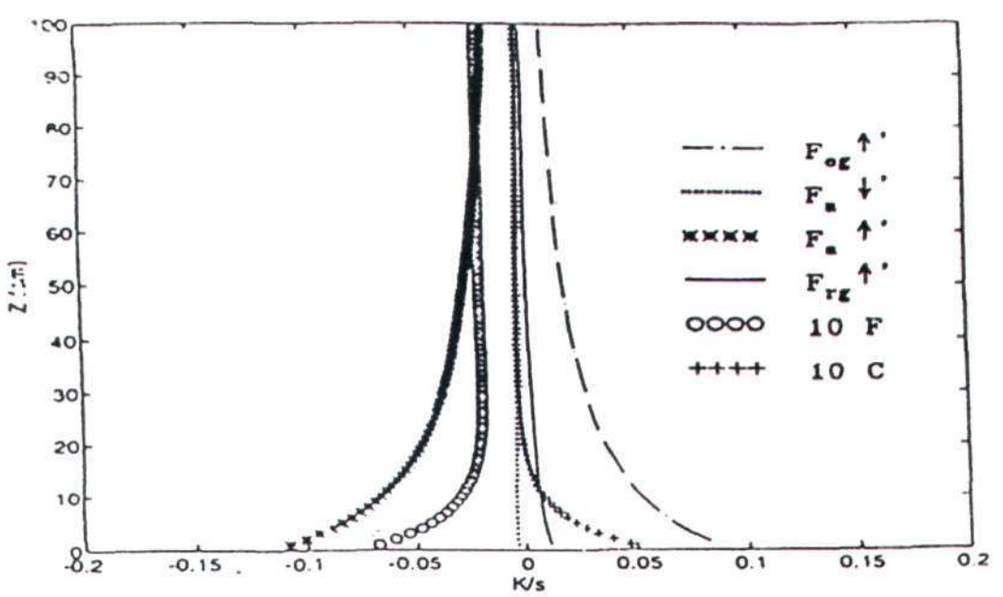

Figure 2.9. Different terms contributing to the energy budget near ground, as a function of height for case III (R.Narsimha and A.S.Vasudevmurthy [1995]).

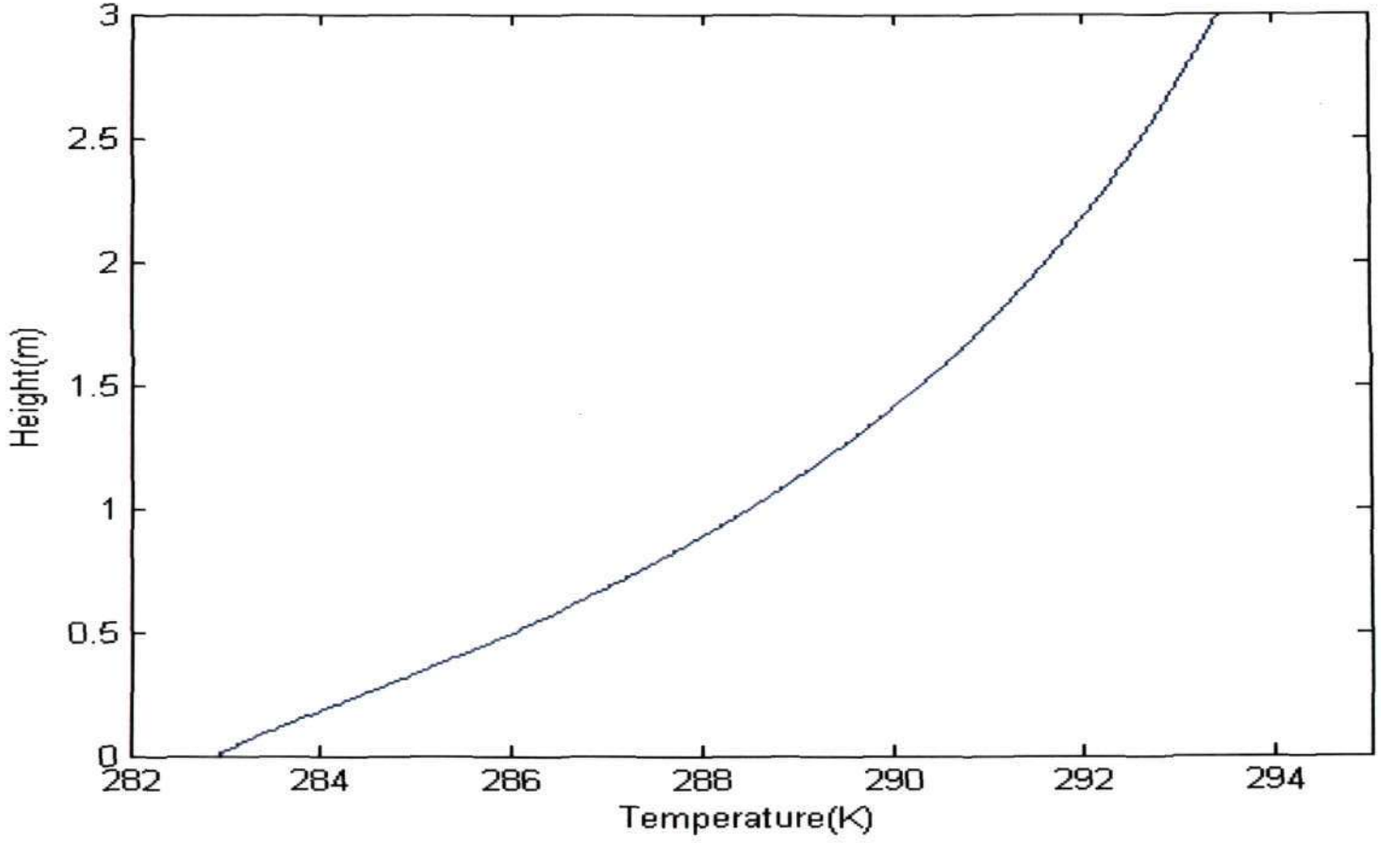

Figure 2.10. Temperature profile for case III.

2.4 Numerical simulation for the lab scale model

In this section we present the details of numerical simulations for the lab scale model. Main objective behind the numerical simulation of the lab model is to see the feasibility of reproducing the LTM under the lab conditions and to decide the parameters that could influence the phenomenon. The governing equations and numerical methodology are the same as in section 2.1 and 2.2. and initial conditions and boundary conditions were changed according to the experimental setup. Experimental setup is shown schematically in Figure 2.11. The experimental setup is discussed in greater detail in Chapter3.

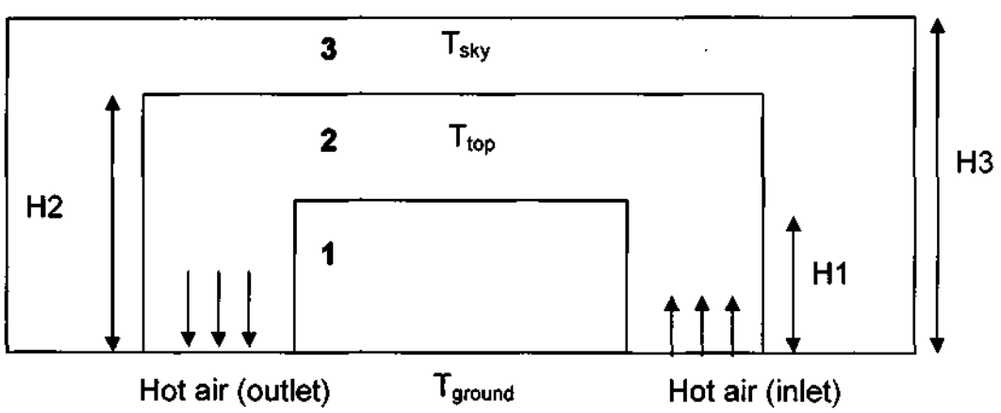

Figure 2.11 Schematic of lab setup

Schematic above shows three regions. Inside the region 1 (test section in the experimental setup) we should get LTM kind of temperature profile, region 2 (air circulation region in the experimental setup) gives the top boundary condition, which decouples the radiative and convective boundaries, and region 3 (outer unit in experimental setup) represents outermost sky at low temperatures. In the centre of the test section, the problem can be treated as one dimensional to a good approximation. This simplified situation is depicted in Figure 2.4.2. Here, the three regions mentioned above, are treated as plane parallel. Bottom boundary has a uniform temperature T_{ground} and outer most boundary has uniform temperature T_{sky}, region in between two middle boundaries

has a uniform temperature T_{top} throughout this region. Inside the region 1, q (the water vapor mixing ratio), has been taken as constant, while in the other two regions this is taken as zero in all the simulation for the lab scale.

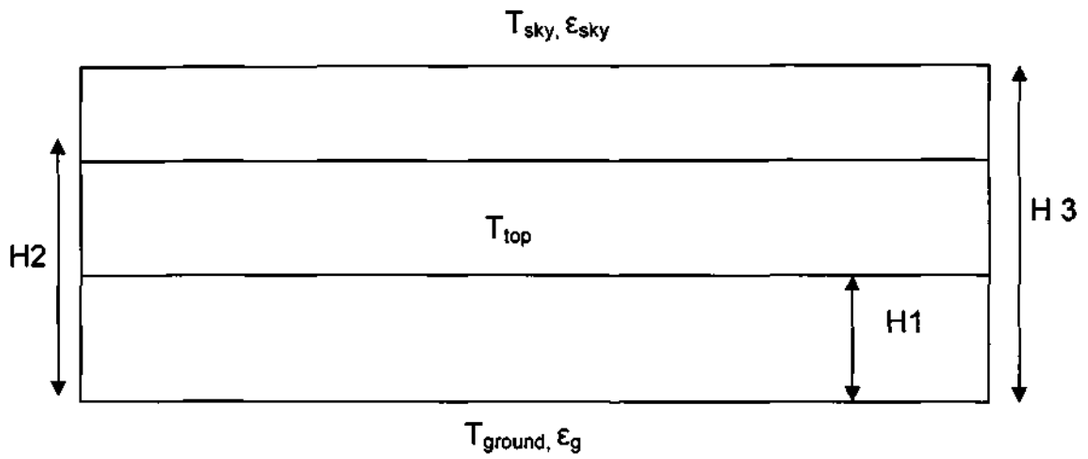

Figure 2.11 Schematic of simplified lab setup (computational domain)

Initial conditions:

$$T(z,0) = T_g \quad \text{for } 0 \le z < H1$$
$$= T_{top} \quad \text{for } H1 \le z \ 0 \le H2$$
$$= T_{sky} \quad \text{for } H2 < z \ 0 \le H3$$

Boundary conditions:

$$T(0,t) = T_g \quad \text{at } z = 0$$
$$= T_{top} \quad \text{for } H1 \le z \le H2$$
$$= T_{sky} \quad \text{at } z = H3$$

2.4.1 Results (unstable stratification)

In this section we have presented the temperature profiles from some initial simulations with unstable stratification in the region1 (test section). Note that we are not accounting for convective transport in our model.

Case 1:

T_g = 360 K; T_{top} =330 K; T_{sky} =270 K;

q = 0.005 (in region1, 0 everywhere else); ε_g=0.8; ε_{sky}=1;

Figure 2.12 shows the complete temperature profile for the whole domain, while Figure 2.13 shows the temperature profile for region 1 mentioned above. Here we can see the effect of radiative cooling clearly, and temperature minimum is at some height above the ground. The results from this simulation show that LTM can indeed be reproduced in the lab provided that the above temperatures and other conditions can be achieved in the lab. But achieving a temperature as high as 360 K for T_g and as low as 275 K for T_{sky} was difficult in the lab with the facilities at our disposal. Hence, we have to check if we can get LTM for the temperatures which can be achieved in the lab.

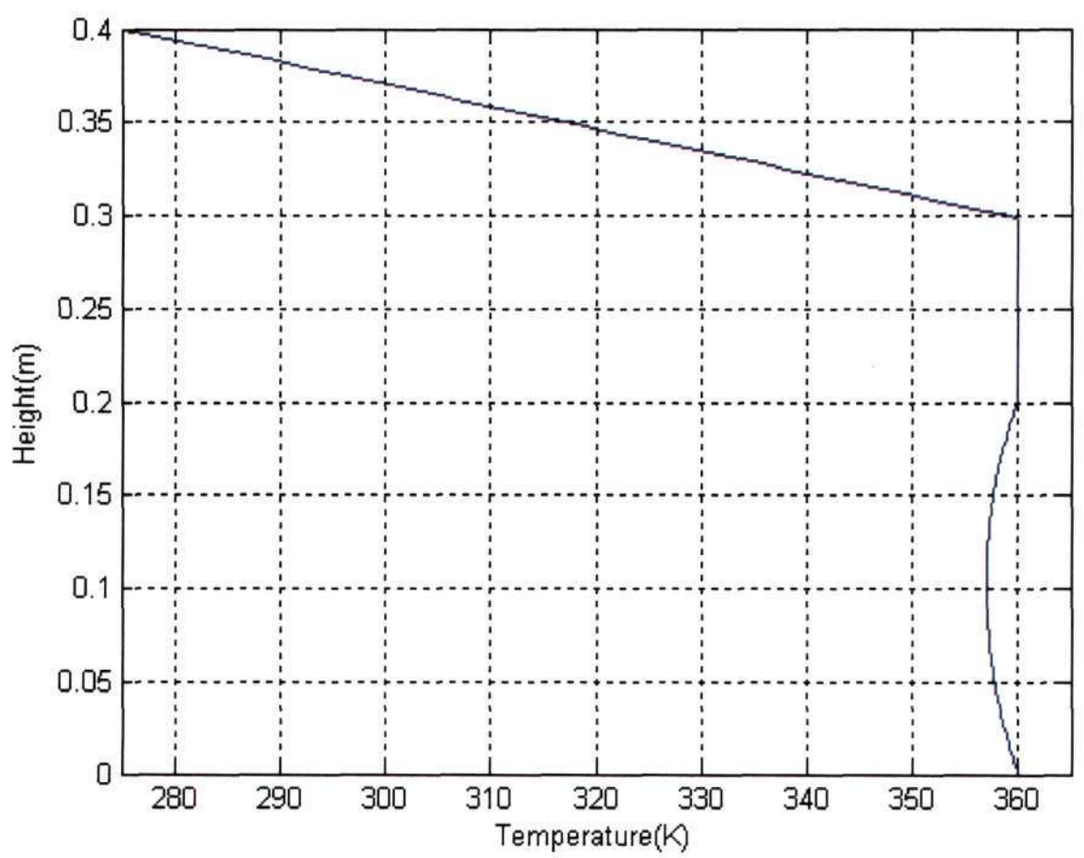

Figure 2.12 Temperature profile for Case1

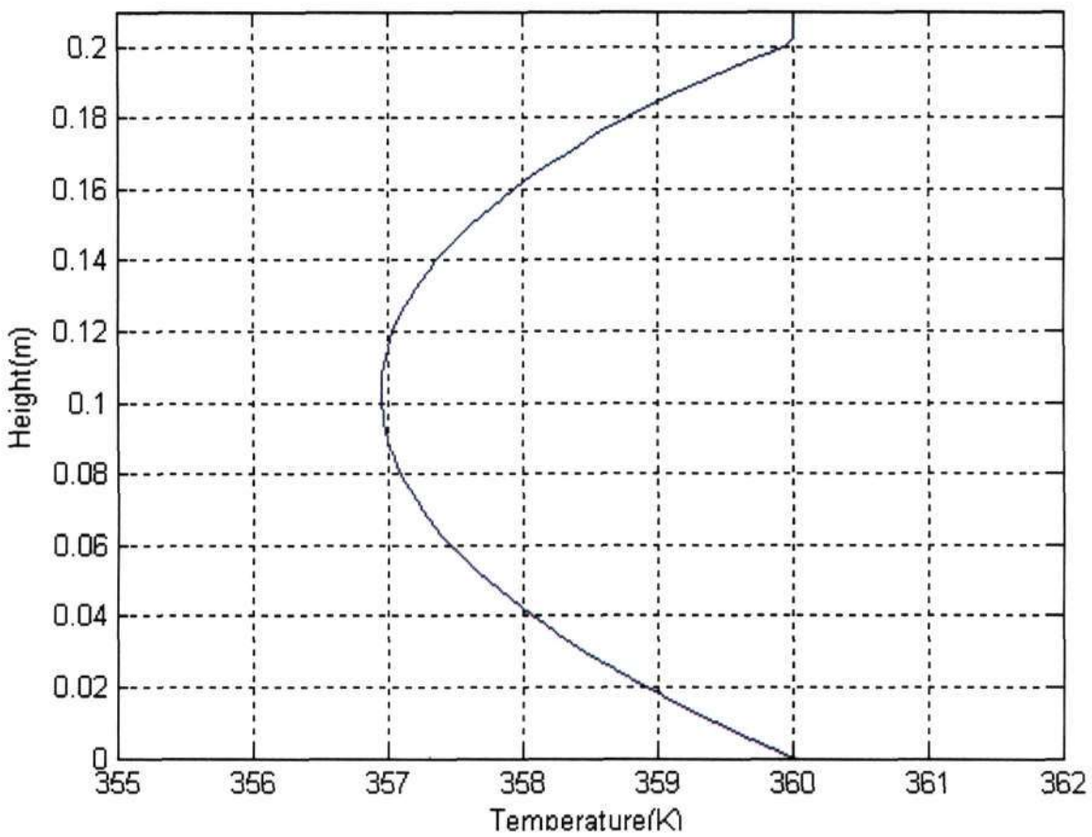

Figure 2.13: Temperature profile for Case 1 (zoomed view)

In case2, we have the boundary temperatures of the range achievable in the lab. Figure 2.14 shows the temperature profile for the whole domain while temperature profile in the test section is shown in figure 2.15. We can clearly observe that minimum appears for these boundary values also hence, it seems that it is possible to reproduce LTM at lab scale.

Case2:

$T_g = 310$ K; $T_{top} = 310$ K; $T_{sky} = 290$ K;

q =0.005 (inside the region1, 0 everywhere else); $\varepsilon_g = 0.8$; $\varepsilon_{sky} = 1$;

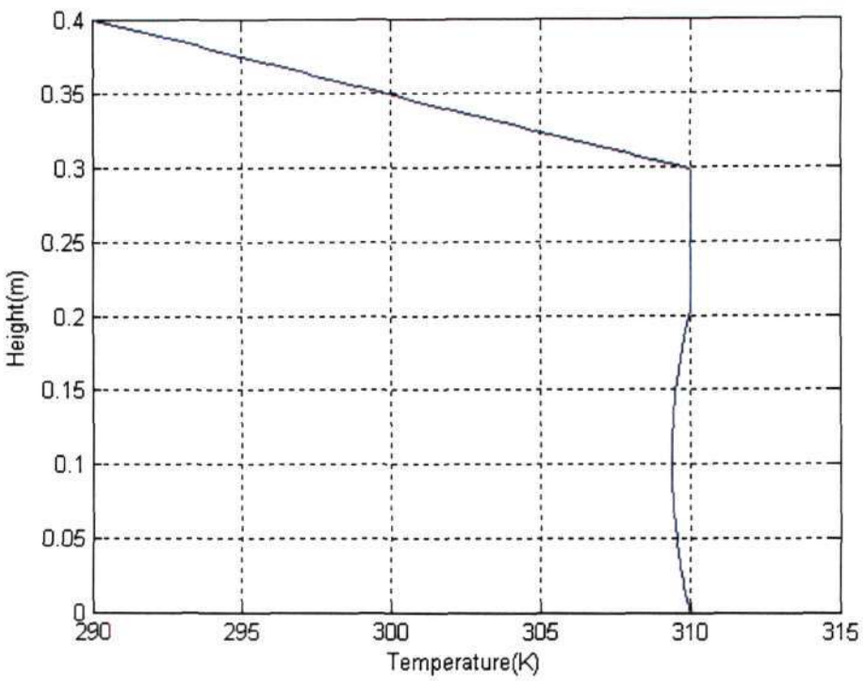

Figure 2.14. Temperature profile for Case 2

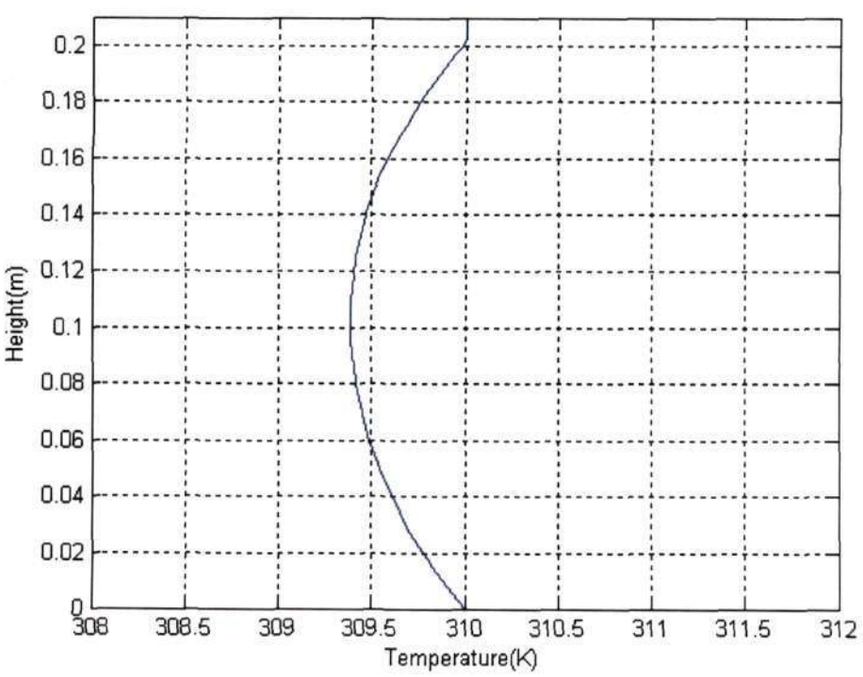

Figure 2.15. Temperature profile for Case 2 (zoomed view)

2.4.2 Results (stable stratification)

It would be interesting to see that what will be the effect of radiation on the temperature profiles when there is stable density stratification in the test section. This configuration helps to highlight the effect of radiation in the absence on convection. Hence, we did numerical simulations for the following three cases with stable stratification in the region1 (test section).

Case1: $T_g = 295$ K; $T_{top} = 300$ K; $T_{sky} = 300$ K; $q = 0.04$; $\varepsilon_g = 0.1$; $\varepsilon_{sky} = 1$;

Case2: $T_g = 295$ K; $T_{top} = 300$ K; $T_{sky} = 300$ K; $q = 0.02$; $\varepsilon_g = 0.1$; $\varepsilon_{sky} = 1$;

Case3: $T_g = 295$ K; $T_{top} = 300$ K; $T_{sky} = 300$ K; $q = 0.04$; $\varepsilon_g = 0.7$; $\varepsilon_{sky} = 0.7$;

Figures 2.16, 2.17 and 2.18 show the profiles of deviations of temperature from linear conductive profile ($T - T_{conductive}$) for the above three cases. All these temperature profiles show that heating is taking place in the lower part of the region1 while cooling is taking place in the upper part of the region1. Results are similar for all the three cases mentioned above. The cross over height (height at which conductive profile crosses the radiative profile) Z_c is 0.0937m, 0.094m and 0.084m for the Case1, Case2 and Case3 respectively.

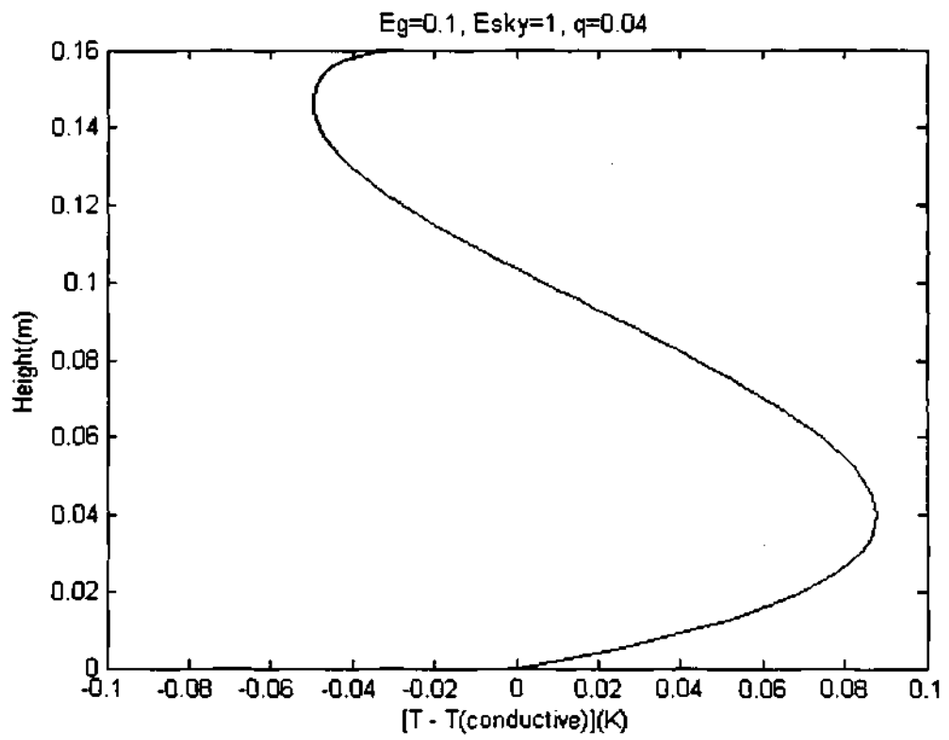

Figure 2.16. Temperature deviation profile for stable stratification (Case1)

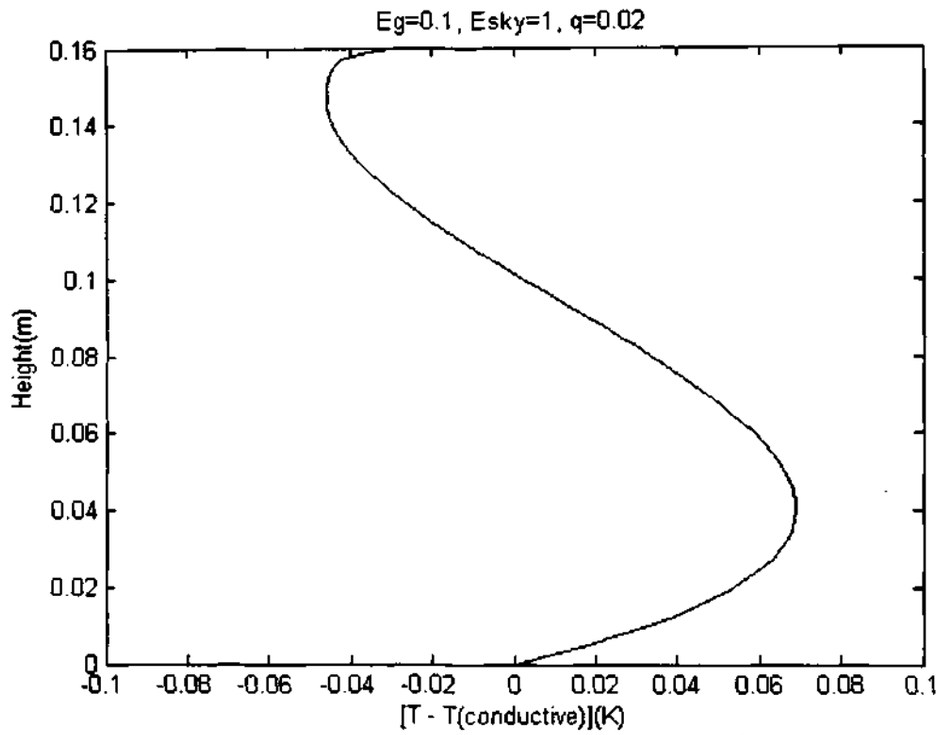

Figure 2.17. Temperature deviation profile for stable stratification (Case2)

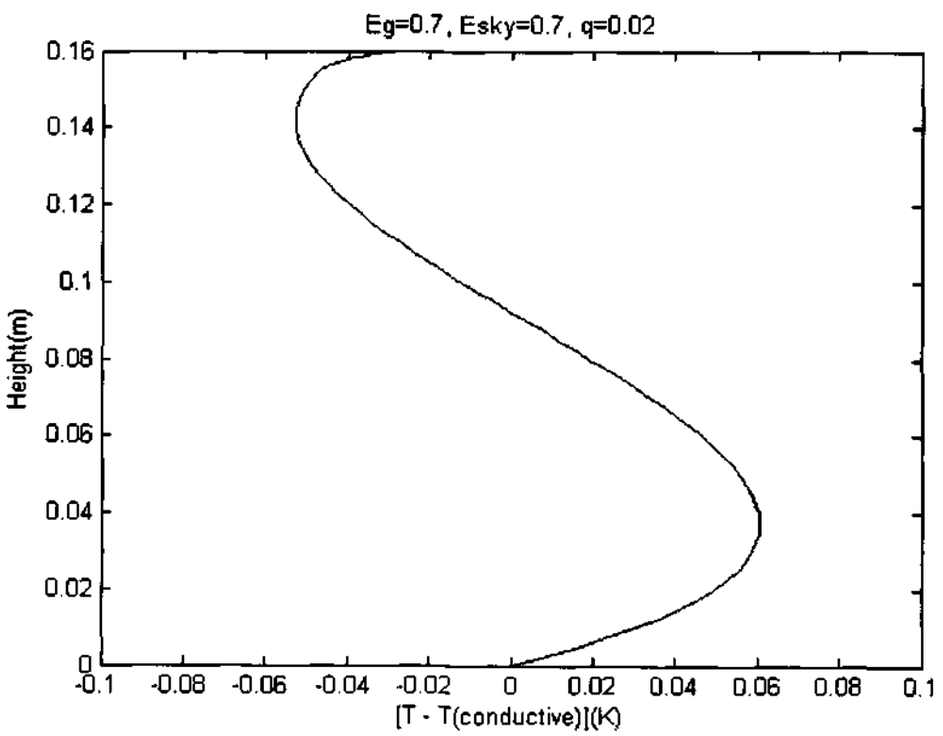

Figure 2.18. Temperature deviation profile for stable stratification (Case3)

Chapter 3 Experiments: Details and specifications

In this chapter, details of the experimental setup and experiments are presented. This chapter is divided into three sections. In section 3.1, the need for a lab simulation is discussed. A basic idea that would enable one to simulate the phenomenon in the lab is also presented. In section 3.2 the experimental setup and its various components are explained in detail. The results for different boundary conditions are presented in section 3.3.

3.1 Design of experimental setup

"Lifted temperature minima" occur in the nights and only in calm and clear sky conditions. Because of these conditions, field experiments can be performed only during nights and during few months in a year. Moreover, in field experiments parameters can not be varied independently, as we do not have much control over the conditions in the field. Therefore, it would be ideal to do the experiments in the lab, so that experiments can be performed at any time of the day and during any period of the year. Moreover, in the laboratory, phenomena can be studied under controlled conditions and parameters can be varied independently. Hence, in order to analyze "Lifted temperature minimum" in a better manner, it is necessary to build a laboratory model. In order to reproduce the LTM in the lab, our experimental setup should mimic the actual situation in which phenomena occurs.

The ground, outer space and the radiatively participating and non-participating atmosphere should be represented by some means in the lab.

Figure (3.1) represents the situation in which phenomena occurs in the field. In this situation, it is the inversion layer above, which a lot of large-scale convection occurs, but it gives a kind of boundary condition, below which convection is less. In the laboratory setup we should have a boundary by some means, which can reduce convection and gives a boundary to decouple the radiative and convective boundaries. A rough schematic of the lab setup is shown in Figure3.2.

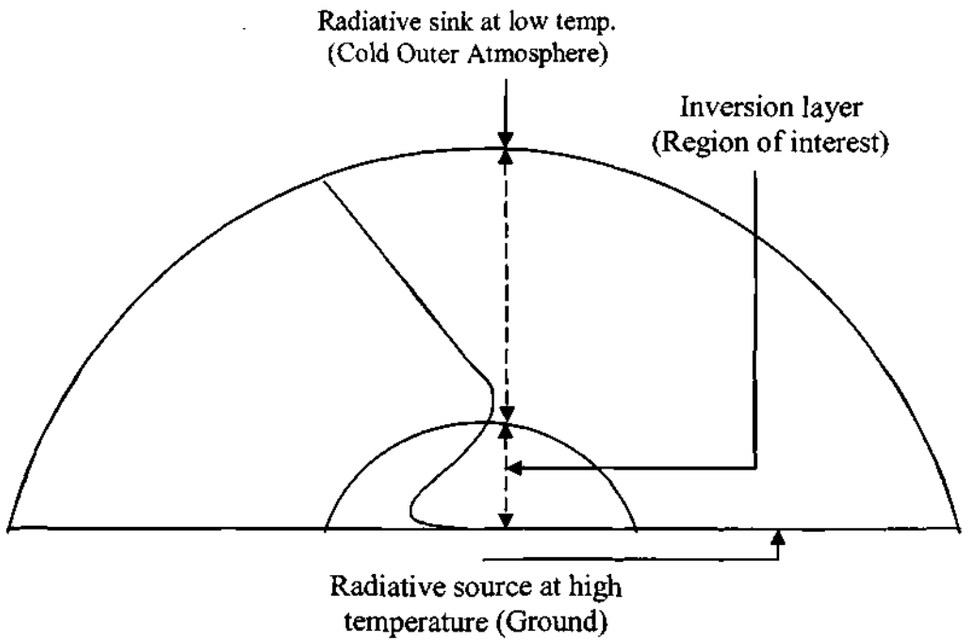

Figure3.1. Actual atmosphere

3.2 Components of lab model

3.2.1 Bottom unit

In the laboratory setup we should have a bottom unit, which represents earth. During the night hours earth acts as a radiative source with higher temperature than the outer sky and radiatively cools to it. Hence we should have a heating unit, which can maintain the temperature of this symbolic ground. Figures 3.3 a, b and c show the details of the bottom unit. To fabricate this unit we have a tank of dimensions (800mm X 800mm X 100mm). Water or any other liquid can fill this tank. To control the temperature of this liquid, copper tubes are placed in the tank. Temperature of the liquid can be controlled by re-circulating hot or cold water in the Copper tubes. On top of the copper tubes an anodized aluminum plate of dimension (800mm X 800mm) is placed, which is always in contact with the liquid in the tank. The liquid inside the tank acts as an intermediate agent for heat transfer. It helps in attaining a uniform temperature

throughout the surface of the top plate. Hence temperature of aluminum plate can be controlled by this arrangement. Sidewalls and bottom of the tank are insulated using a layer of Glass wool to minimize heat loss to the surroundings.

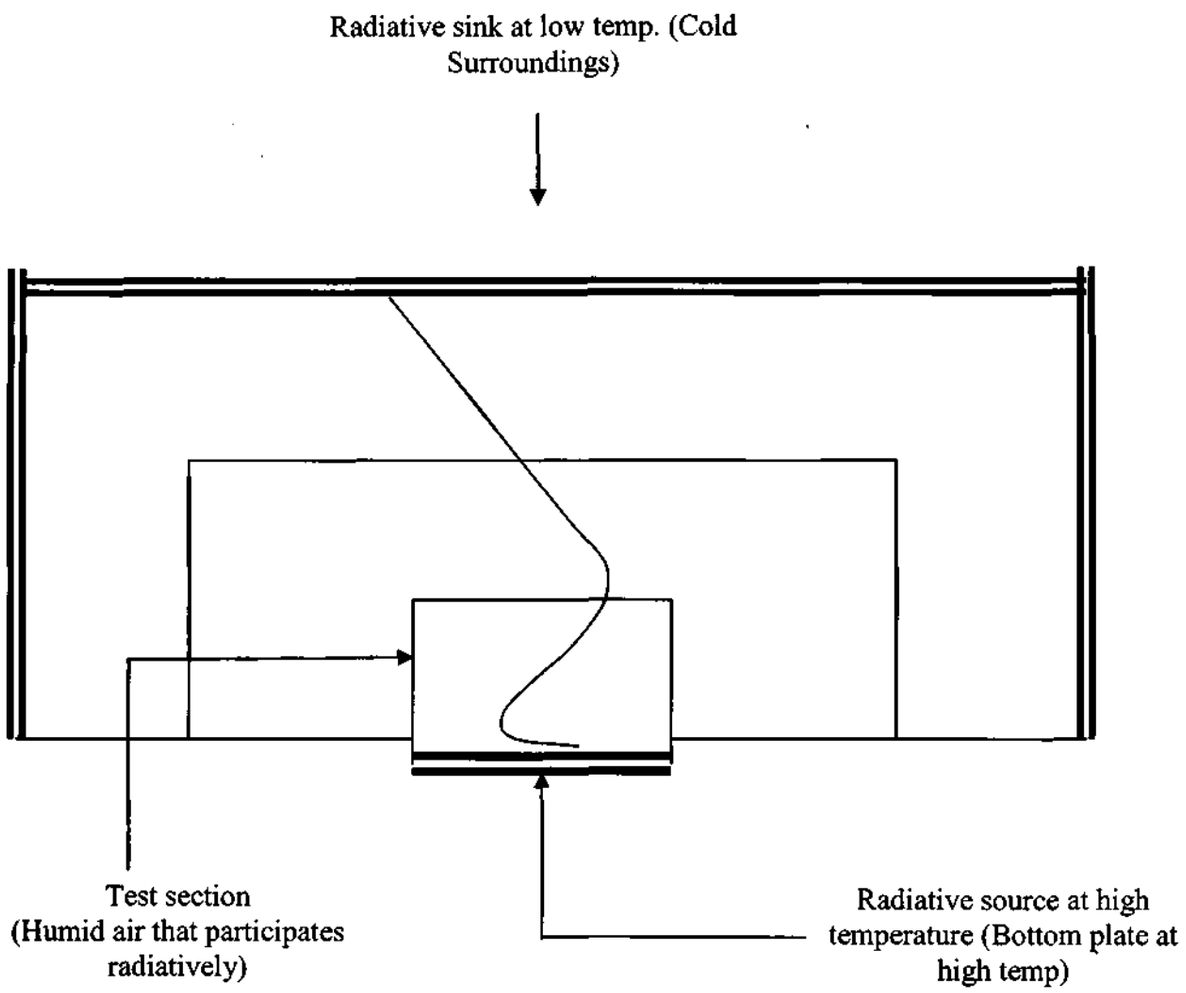

Figure3.2. Rough schematic of Experimental setup

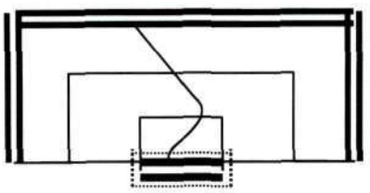

(a) Bottom unit, highlighted by dotted lines

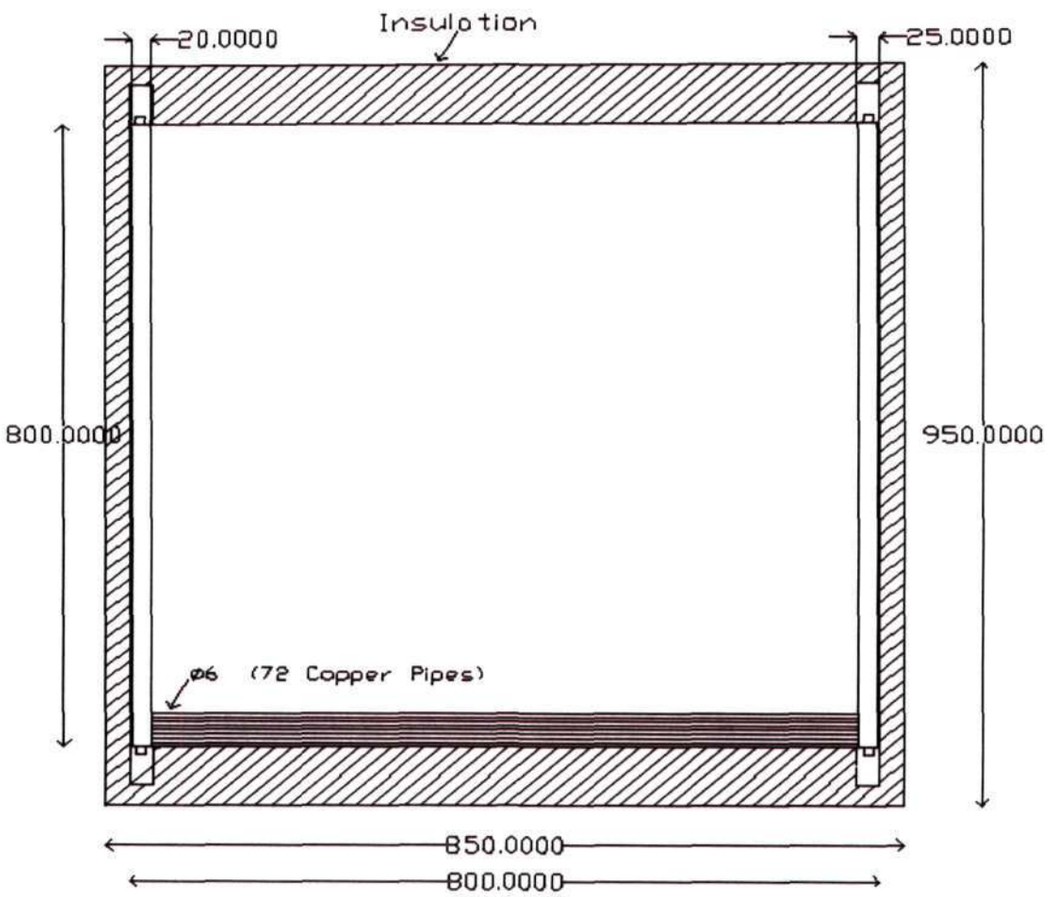

(b) Top View

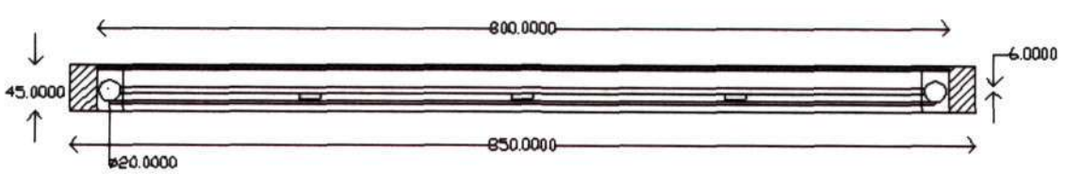

(c) Front view

Figure 3.3. Bottom unit

3.2.2 Test section

This is the section where all temperature measurements are done. In actual situation this mimics the air layers very near the ground. Inside this section atmospheric air (or any other gas with known properties) can be used as test gas. Boundaries of the test section should be such that, it should be transparent to the radiation and it should not let the gas to leak (convection should not happen). Figures 3.4 a and b show the details of the test section. To fabricate this region, a cuboidal iron frame is made of dimensions (900mm X 900mm X 210mm). On this frame, thin polythene sheets were rapped to make the walls of the iron frame. To select the polythene sheets for the setup, we measured transmissivity of different samples available and used the sample, which had the highest transmissivity (90%) for most of the infrared region. In Appendix I transmissivity of different samples are plotted.

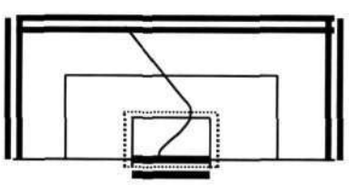

(a) Test section, highlighted by dotted lines

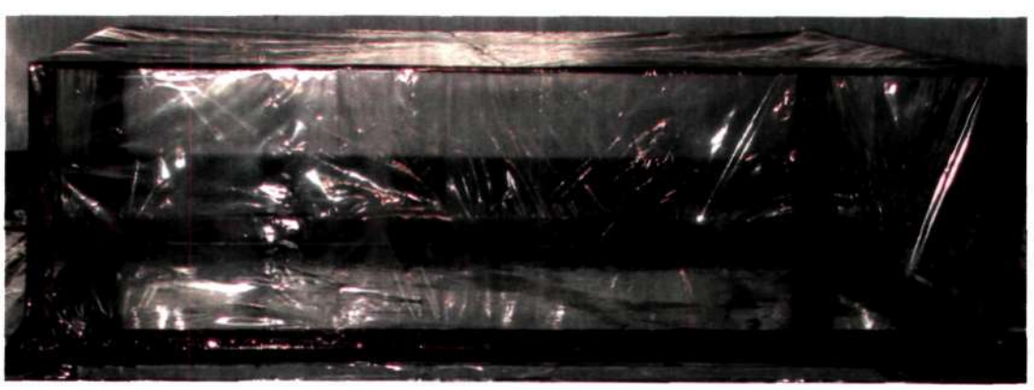

(b) Actual picture of the test section

Figure 3.4. Test section

3.2.3 Air circulation unit

Above the test section we have a region in which dry air is to be circulated. The temperature of the air can be controlled through a heater-blower unit. This is the region, which provides the desired boundary condition at the top of test section. Dry air is used because it is transparent to radiation. Figures 3.5 a and b show the details of the air circulation unit. To fabricate this region a cuboidal iron frame is made of dimensions (900mmX900mmX400mm). On this frame, walls are made of thin polythene sheets. To circulate the air uniformly in this region, inlet of the air is first opened into a box and from there it is allowed to enter this region. This box is tightly packed with straws. Hence, after the box, air has to pass through these straws to enter the air circulation region. Similar set up is made at the other end for outlet of air. This makes sure that circulation of the air is uniform throughout the chamber.

3.2.3.1 Heater-blower unit

Figure 3.6 shows a heater blower unit. Temperature of the air was increased by using two such units. A fan was used to blow the air to a pipe of diameter 6cm. Inside the pipe an electrical heating element is fitted. By blowing the air on heating coils temperature of the air can be increased significantly. Output temperature of the air is controlled by changing the input voltage to the heating coils.

3.2.4 Outer unit

Figures 3.7 a, b and c show the details of outermost sky. Outer most sky is simulated by having a cold surface surrounding the recirculation region. This is achieved by having the four sides and the top form an enclosure whose temperature is lower than that of the bottom. Four Aluminum boxes of size (1600mmX80mmX1000mm) are made which are placed as four outer walls of the whole setup. These boxes rest on four stands horizontally in level with central bottom plate. To decrease the temperature of the walls, these boxes are to be filled by cold water (ice-water mixture). For further control of the temperature of water, copper tubes are place inside the tanks and any hot or cold fluid can

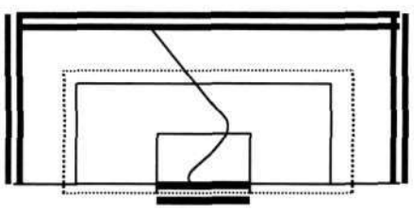

(a) Air circulation unit, highlighted by dotted lines

(b) Actual picture of the air circulation unit

Figure 3.5. Air circulation unit

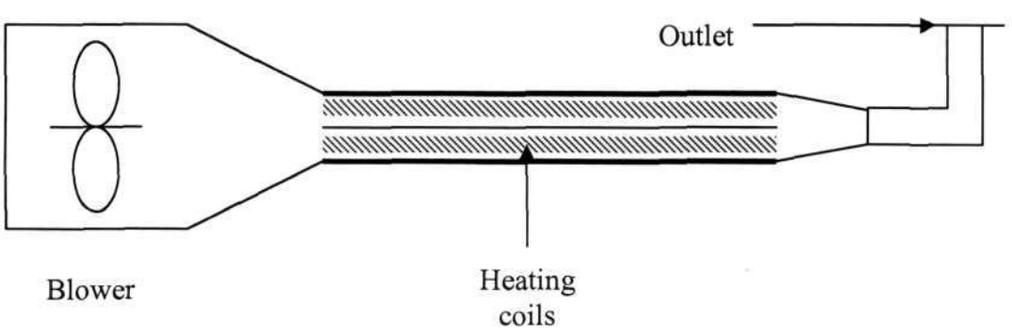

Figure 3.6. Heater blower unit

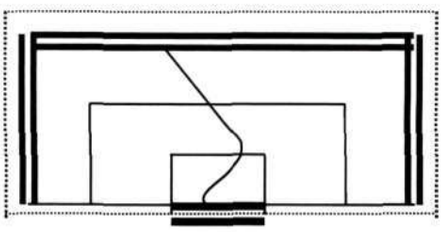

(a) Outer unit, highlighted by dotted lines

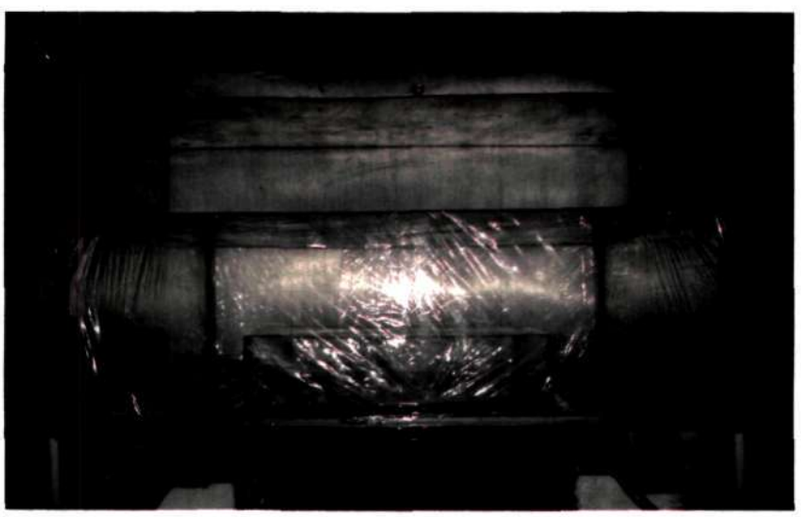

(b) Actual picture of outer unit, taken from inside the setup

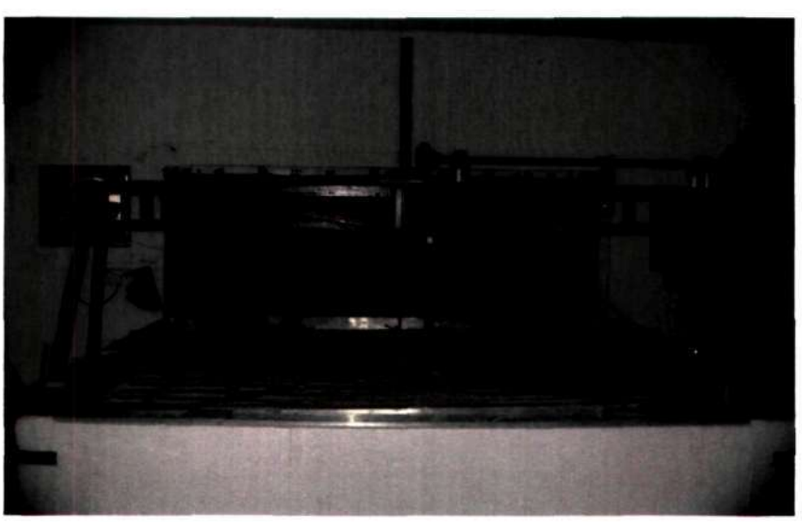

(c) Arrangement to change height of top outer unit

Figure 3.7. Outer unit

be circulated through the water. Outer walls of these boxes have insulation to prevent heat loss to the surroundings. The top most surface is an Aluminum tank with dimensions (1000mmX1000mmX90mm). This tank hangs through a pillar. The height of the tank can be changed by a Bevel gear and screw arrangement. This tank can be filled by cold water (ice-water mixture) and to maintain and control the temperature, copper tubes are placed inside the tank through which hot or cold fluid can be circulated.

3.3 Results

All the experiments done are tabulated in Appendix II (List of experiments). In this section we present only the significant results.

3.3.1 Unstable stratification

In this section we shall present results of the experiments done with unstable stratification in the test section i.e. hot bottom and colder top.

3.3.1.1 Experiments by traversing the thermocouples

Initial sets of experiments were done by traversing the thermocouples in the test section. Traversing the thermocouple and recording the temperatures to obtain a detailed profile took around 10 minutes. This is a significant amount of time in the sense that, on several occasions, the temperatures at the boundaries changed significantly within one traverse cycle. In spite of some improvements in the setup, the traverse time could not be reduced much. Hence, the traverse method was later abandoned in favor of an arrangement where a rack was used to mount a set of thermocouples at different fixed heights. For completeness, we show in Figure 3.8, results from an experiment in which this method (traverse) was used.

Here continuous line shows the temperature profile in the test section. While other symbols are temperatures at some fixed locations, which are plotted here with height but actually they mean that, what was the temperature at that respective point, when traversed thermocouple was at any particular height. So by this we are basically plotting temperatures of other points as the time is varying. We tried to maintain the temperatures of all the boundaries constant but it was difficult to keep it constant for a large duration.

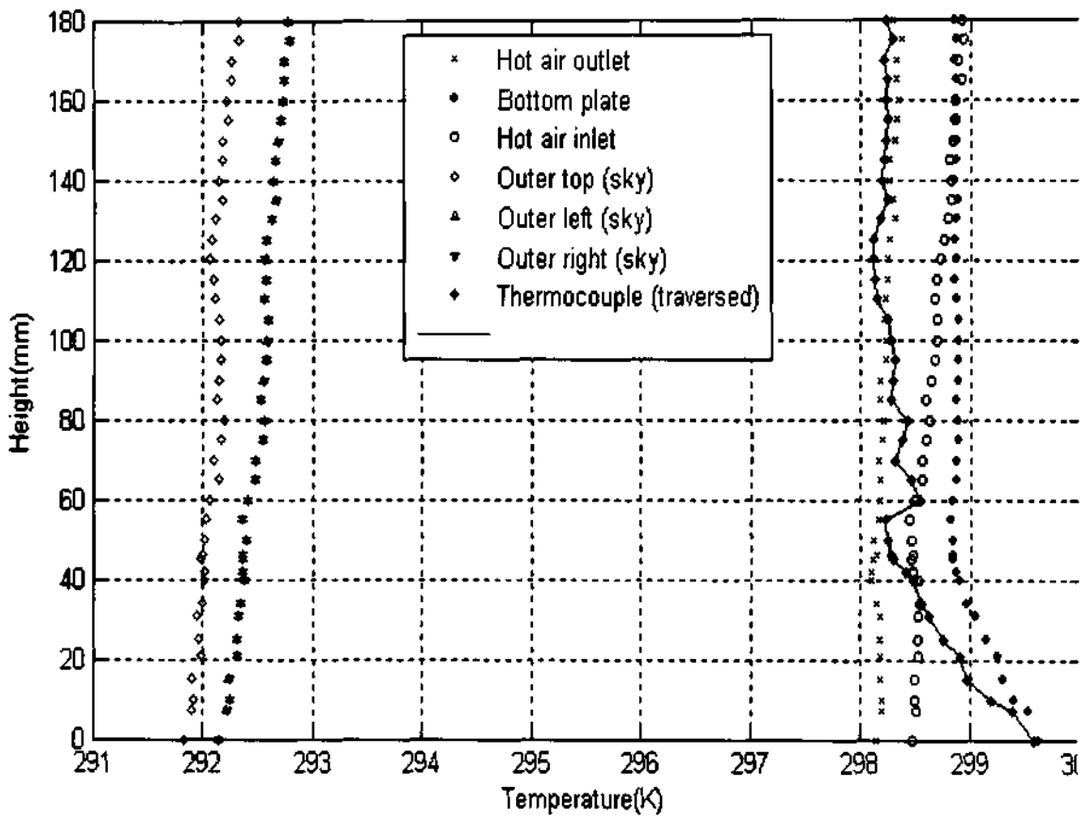

Figure 3.8. Temperature profile by traversing the thermocouple [Exp. # 5]

Since, temperature profile by traversing the thermocouple does not really show the temperature profile in the test section at any particular instant of time, we decided to measure the temperatures in the test section by a rack.

3.3.1.2 Experiments using rack of thermocouples

A rack was fabricated on which thermocouples were placed at heights Z (mm) = [1 2 3 4 6 8 15 30 50 80 110 140 170 190]. Figure 3.9 shows the typical temperature profile for unstable stratification in the test section. Qualitatively temperature profiles are similar in most of the experiments. In the lower part of the test section we see a LTM kind of temperature profile but in the upper part temperatures are fluctuating. In all theses experiments we have maintained an unstable density gradient, as temperature is higher at bottom and lower at the top. Hence there is a possibility of convection.

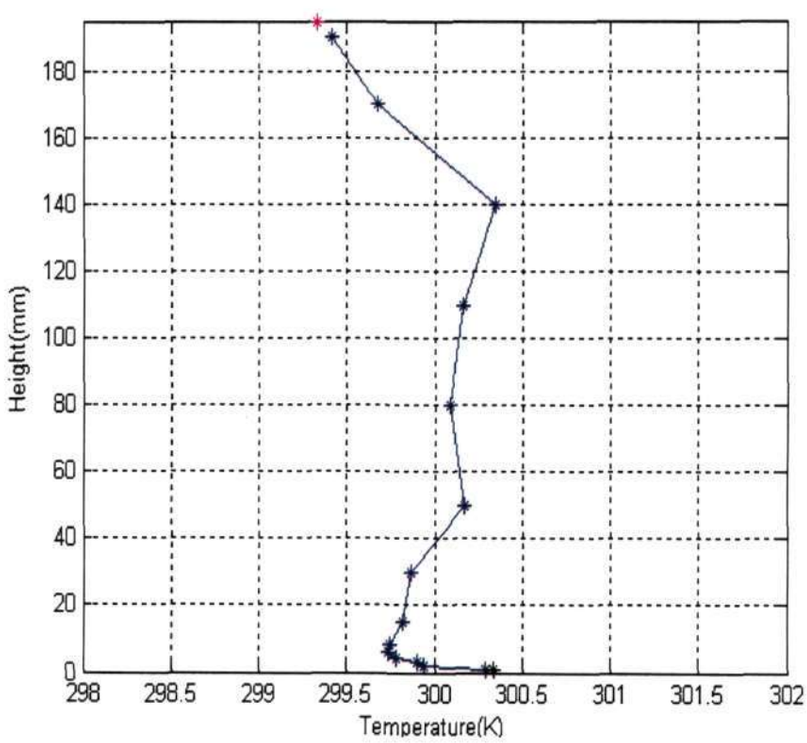

Figure 3.9. Temperature profile using rack of the thermocouple [Exp. # 10]

To understand the dynamics of the phenomena in a better manner, we should have an accurate temperature profile near both the boundaries of the test section.

3.3.1.3 Experiments using rack (high resolution) of thermocouples

A higher resolution rack was needed, as it was necessary to capture the temperature profile near the boundaries of the test section (bottom and top) in a better manner. Hence, a rack was fabricated carefully on which thermocouples were placed at heights Z (mm) = [1 2 3 5 8 15 25 40 55 85 125 155 170 185 195 202 205 207 208 209]. From here onwards we are presenting the results only for the cases where rack with high resolution was used for measuring temperature profile.

Figure 3.10 shows the typical temperature profile for the unstable stratification in the test section. Here filled dots show the temperatures of the fixed thermocouples at bottom plate and top of the test section. In most of the experiments LTM kind of profile is visible in lower part of the test section. Most of the repetitions of the experiments show that profiles are similar in qualitative manner, especially up to the height of 85 mm, shape of the profiles are very much similar to LTM. In the region near the top boundary, temperatures are fluctuating which may be due to the convection. To study the effect of radiative heat transfer alone, it would be necessary if we can make sure by some means that convection is not there. This can be done by maintaining a stable density gradient across the test section (i.e. high temperature at top of the test section and low temperature at bottom of the test section). In that case deviations from the conductive profile will be only due to the effect of radiatively participating medium.

3.3.2 Stable stratification

In this section we present results of the experiments done with stable stratification inside the test section i.e. cold bottom and hot top. The circulation unit and outer unit were at ambient temperature as it was difficult to increase the temperature of the outer unit. Temperature of the bottom plate was decreased to get the stable stratification.

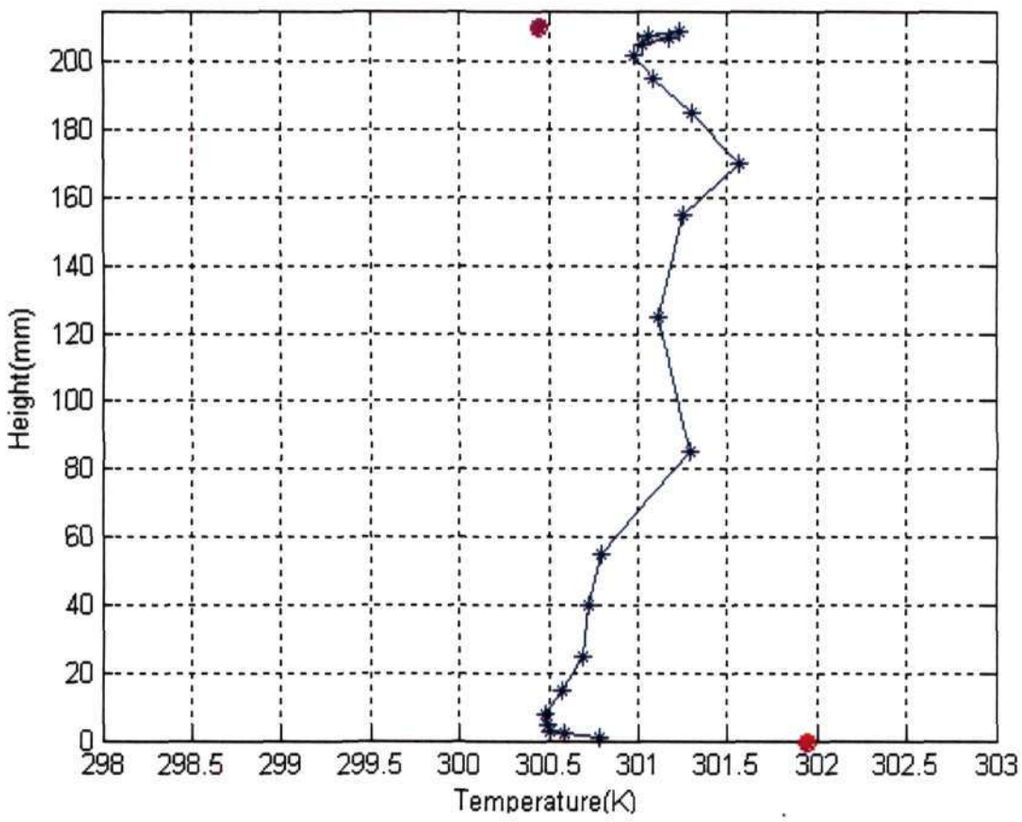

Figure 3.10. Temperature profile using rack of the thermocouple [Exp. # 18]

Effect of changing the temperature gradient, sky temperature (outer unit temperature) and emissivity of the bottom plate, was observed. All the results presented here have been repeated enough number of times to confirm the results. Here also as in the previous sections, we shall present one representative result for each type of experiment. All the experiments for the stable stratification were done with the high-resolution rack. All the experiments done are tabulated in Appendix I (List of experiments).

3.3.2.1 Bottom surface: Reflective (low emissivity)

In this section we present the results for highly reflecting bottom plate (i.e. low emissivity=0.04) of the bottom plate. This was done by sticking a reflective sheet on the bottom plate. Figure 3.11 (a) and (b) show the temperature profiles of the stable

stratification case for different boundary conditions. Filled dots show the temperatures of the fixed thermocouple at bottom plate and top of the test section. All the temperature profiles observed were highly stable and shapes of the profile were qualitatively similar irrespective of the temperature gradient.

3.3.2.2 Bottom surface: Aluminum (moderate emissivity)

In this section we present the results for anodized Aluminum bottom plate (i.e. emissivity=0.77) of the bottom plate. Figures 3.12 (a) and (b) show the temperature profiles of the stable stratification case for different boundary conditions. Filled dots show the temperatures of the fixed thermocouple at bottom plate and top of the test

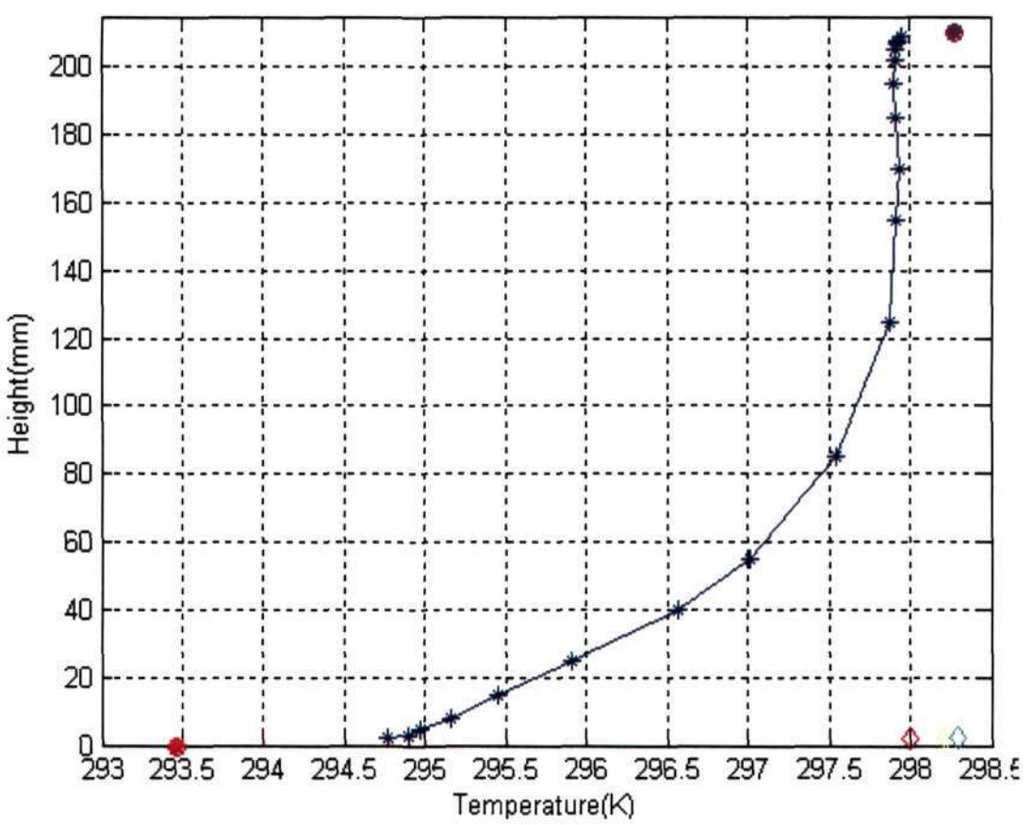

Figure 3.11(a). Temperature profiles (Low ΔT) (Bottom: Reflecting) [Exp. #25]

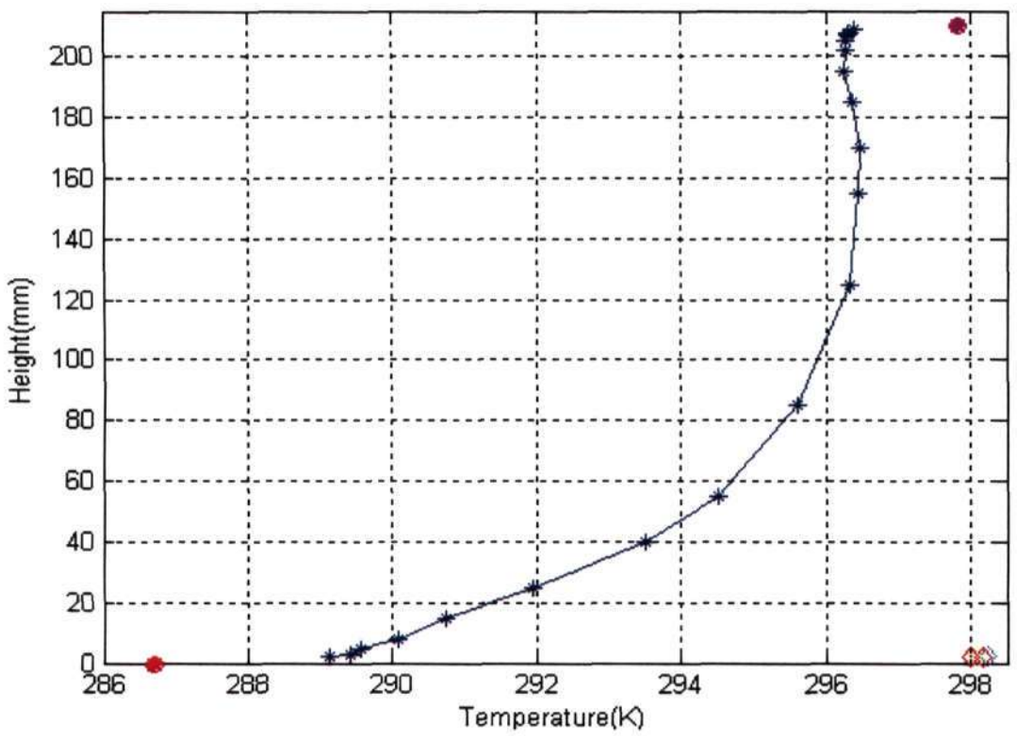

Figure 3.11(b). Temperature profiles (High ΔT) (Bottom: Reflecting) [Exp. # 29]

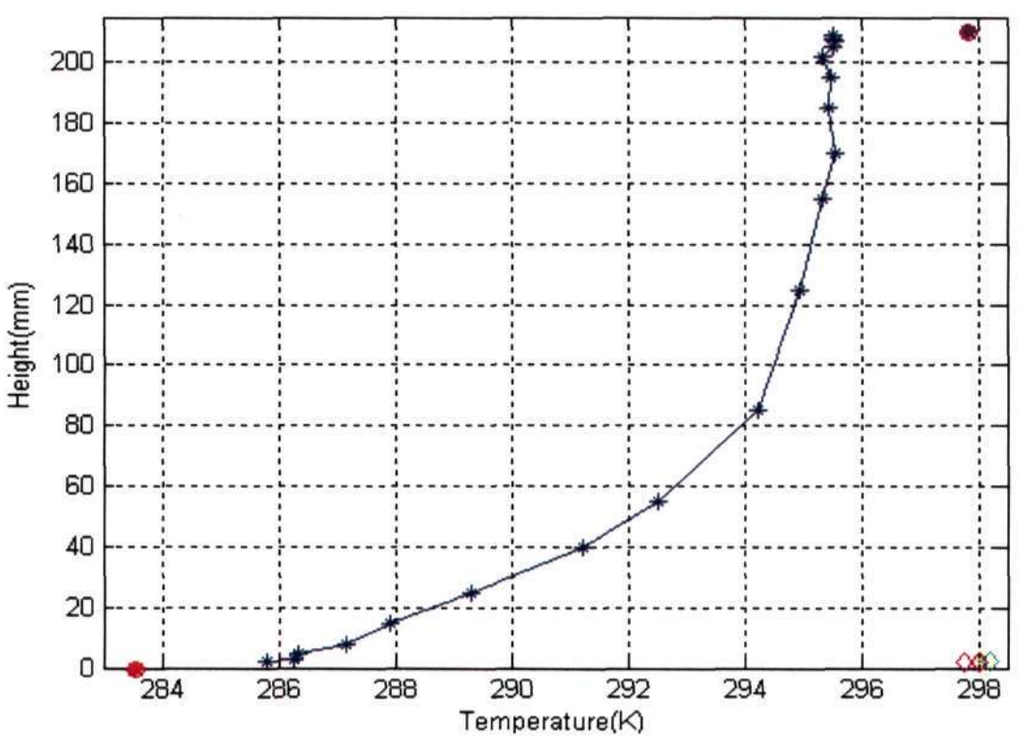

Figure 3.12(a). Temperature profiles (High ΔT) (Bottom: Aluminum)

[Exp. # 35]

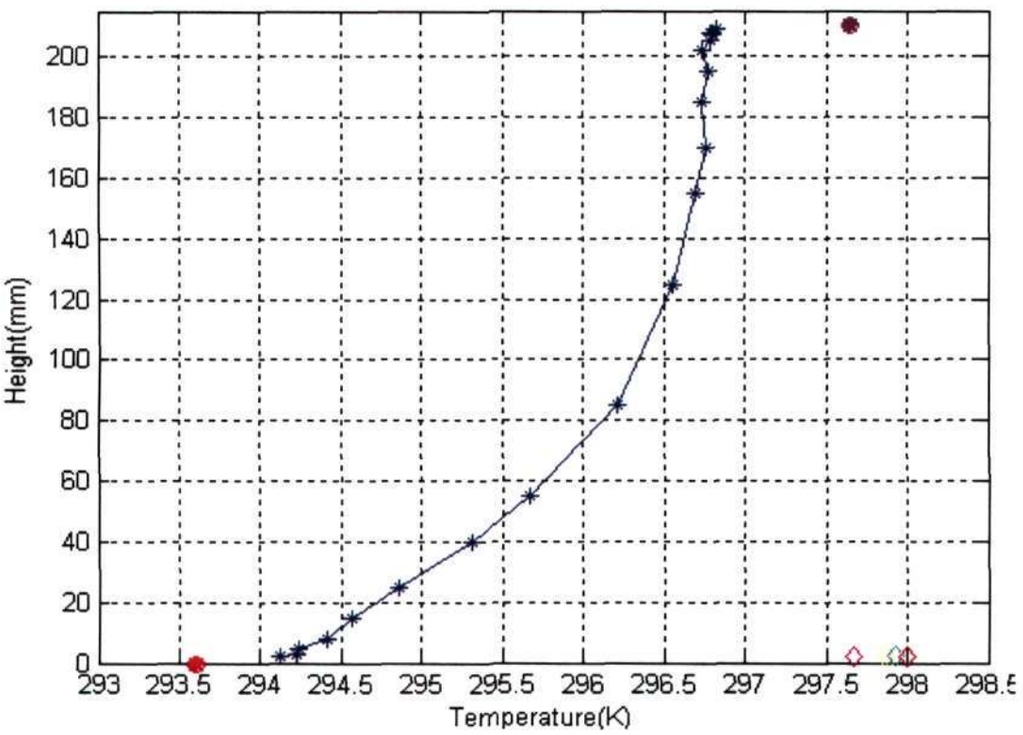

Figure 3.12(b). Temperature profile (Low ΔT) (Bottom: Aluminum) [Exp. # 37]

section respectively. Temperature profiles for most of the experiments show significant deviation from the conductive profile. We don't see any sign of convection from the temperature profiles and in general shapes of the temperature profiles were qualitatively similar for various temperature differences between bottom and top as long as the stratification was stable.

3.3.2.3 Bottom surface: Black (highest emissivity)

In this section we present the results for black bottom plate (i.e. emissivity of the bottom plate ~1). This was done by sticking the black painted polythene sheet on the bottom plate. Temperature profiles for this case are slightly different from the above two cases. Here again we see significant deviations from the conductive profile. Figure 3.13 shows the time series plot for this case. Here Red and Black lines are time series for bottom plate and top boundary respectively while all Blue lines are time series for the in between positions. Looking at the time series plot, we observe an instability which,

appears at a height of 195mm and at time around 500 seconds. This can also be seen from the vertical temperature profiles shown in Figures 3.14 (a), (b) and (c). Starting from the steady state (Figure 3.14 (a)) the instability grows till we see a kink at a height of 195mm (Figure. 3.14 (b)). The temperature profile then stabilizes and steady state is reached again (Figure. 3.14 (c)).

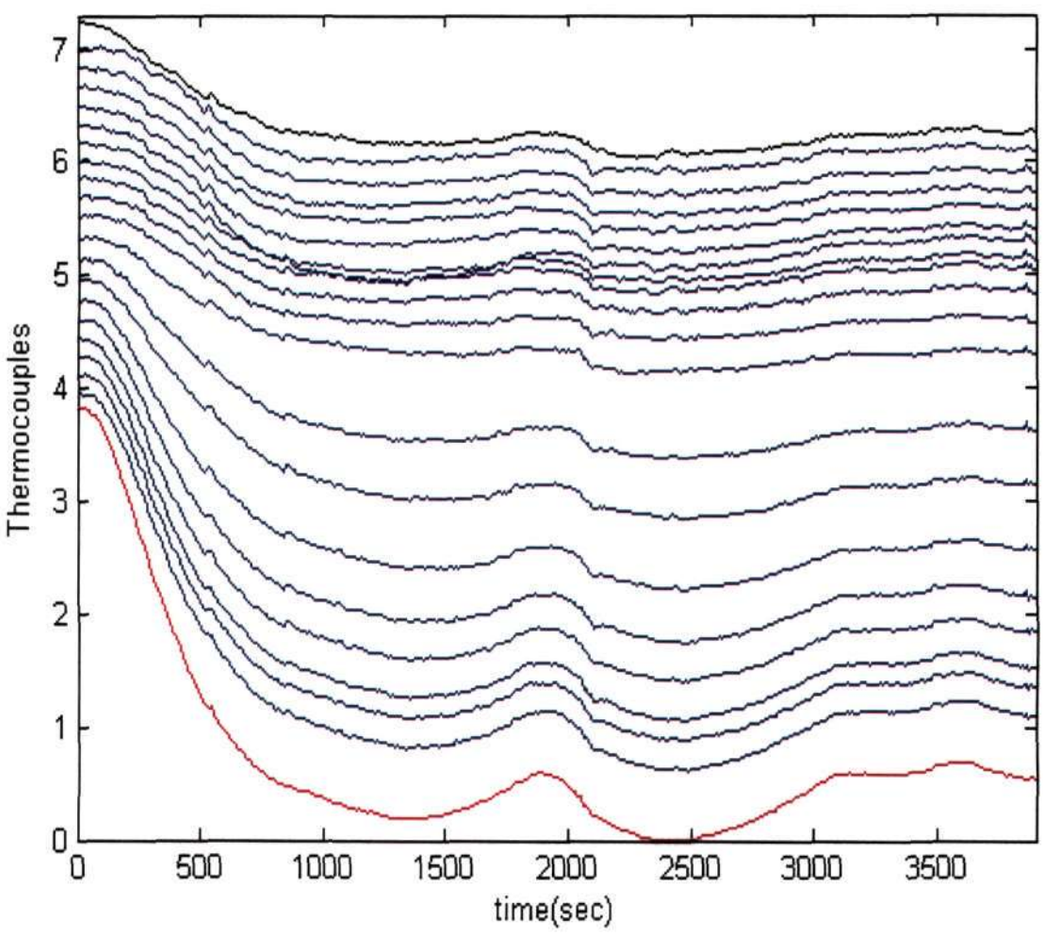

Figure 3.13. Time series (Black bottom) [Exp. # 46]

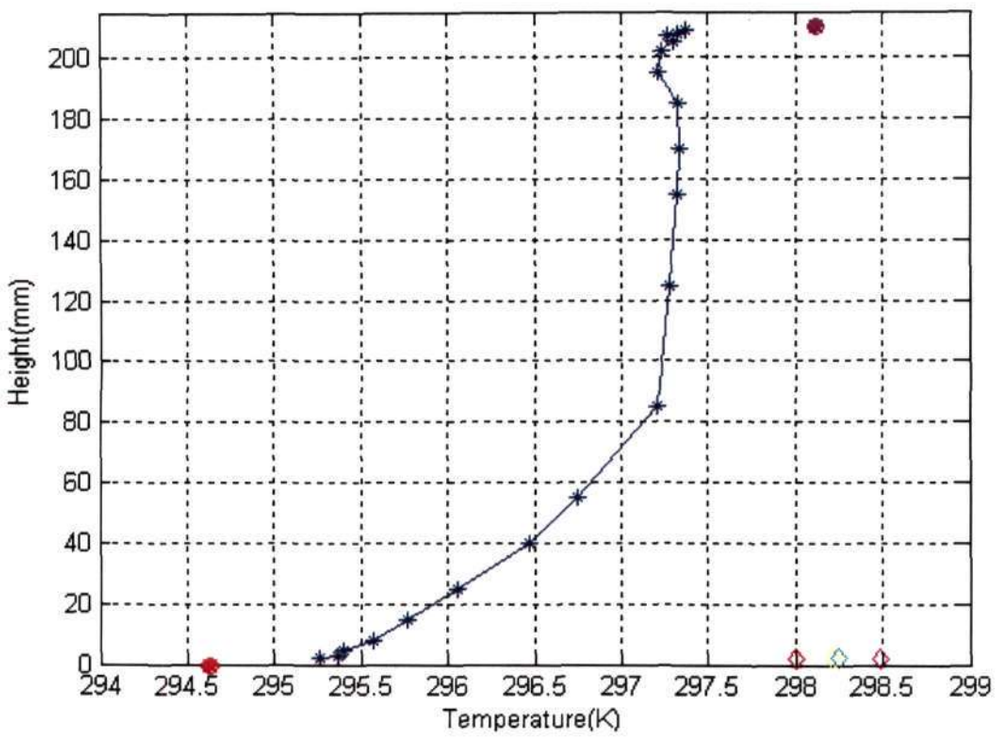

Figure 3.14. (a) Temperature profile (t = 500 sec) (Bottom: Black) [Exp. # 46]

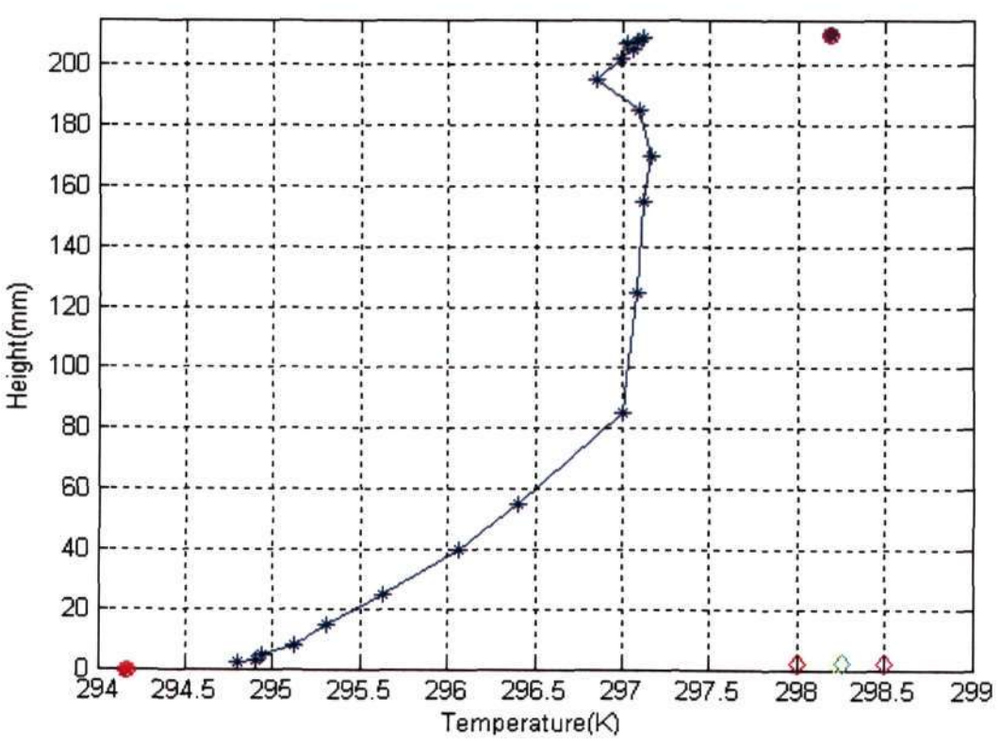

Figure 3.14. (b) Temperature profile (t =1300 sec) (Bottom: Black) [Exp. # 46]

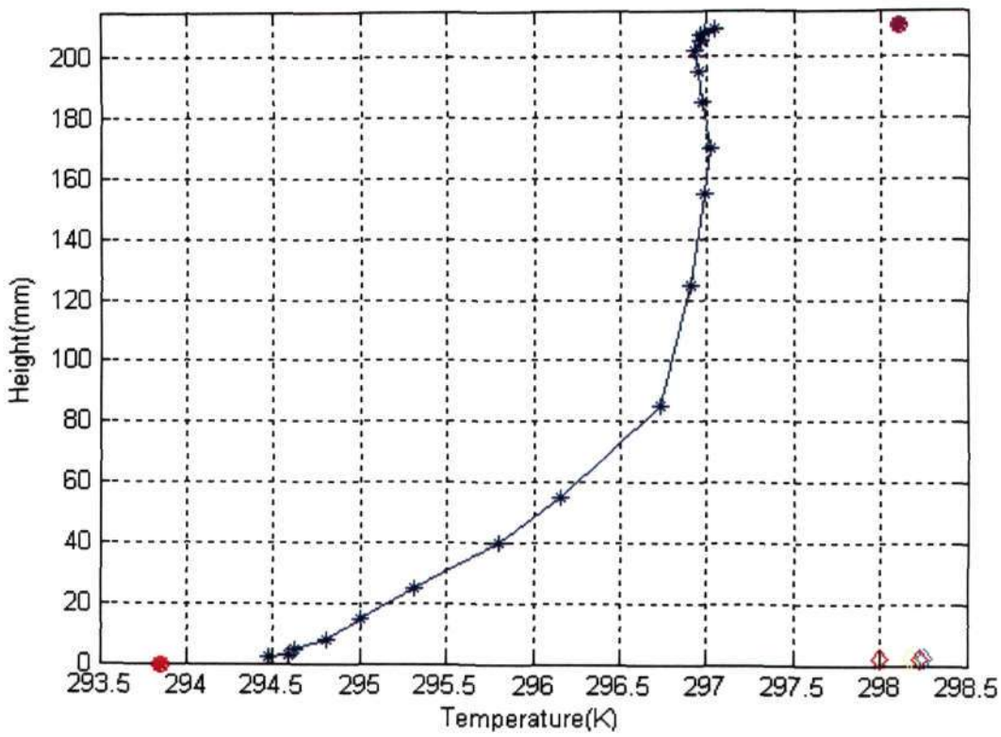

Figure 3.14. (c) Temperature profile (Steady state) (Bottom: Black) [Exp. # 46]

3.3.2.4 Comparative study of changing emissivity of bottom surface

In this section we have compared the results for different emissivities of the bottom plate and plotted the non-dimensional temperatures with non-dimensional heights. Horizontal axis is non-dimensional temperature theta, non-dimensionalized as

$$\text{theta} = (T - T_{bottom}) / (T_{top} - T_{bottom})$$

and vertical axis is non dimensional height H, non dimensionalized as

$$H = Z / H_1 \qquad \text{where} \quad H_1 = \text{Test section height}$$

While Z_c is the height at which experimental profile crosses the conductive profile.

Figure 3.15 shows the non-dimensional temperature profile for reflecting bottom surface.

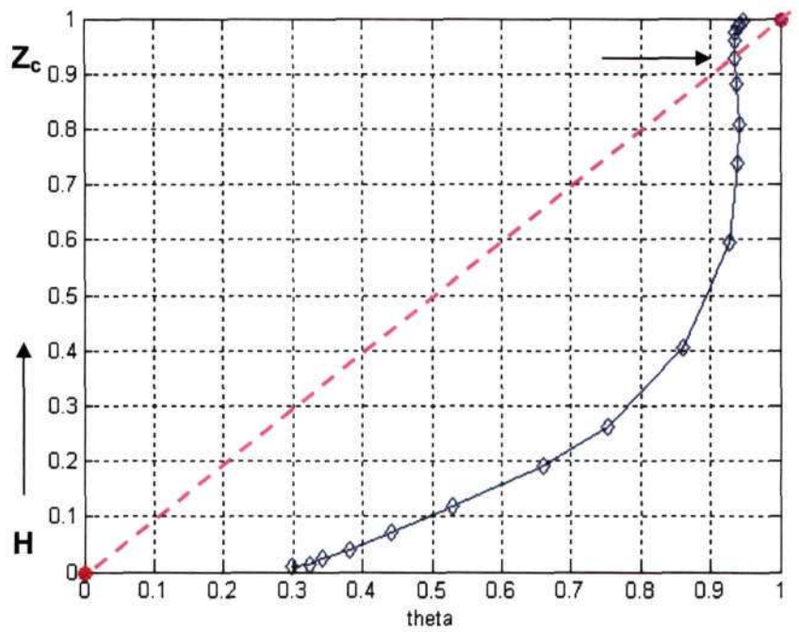

Figure 3.15. Non–dimensional Temperature profile (Bottom: Reflective) [Exp. #29]

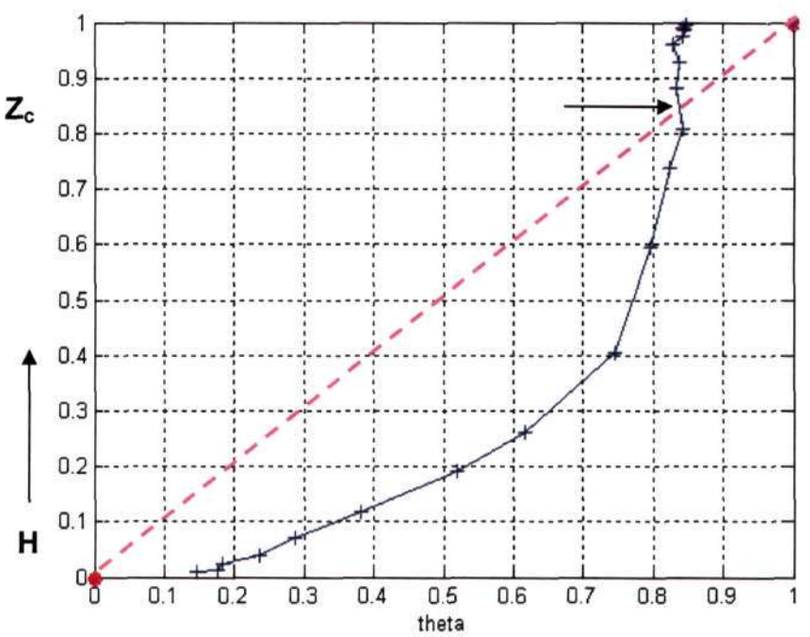

Figure 3.16. Non–dimensional Temperature profile (Bottom: Aluminum) [Exp. # 35]

Figure 3.16 shows the non-dimensional temperature profile for the case where bottom surface was Aluminum.

Figure 3.17 shows the non-dimensional temperature profile for black bottom surface.

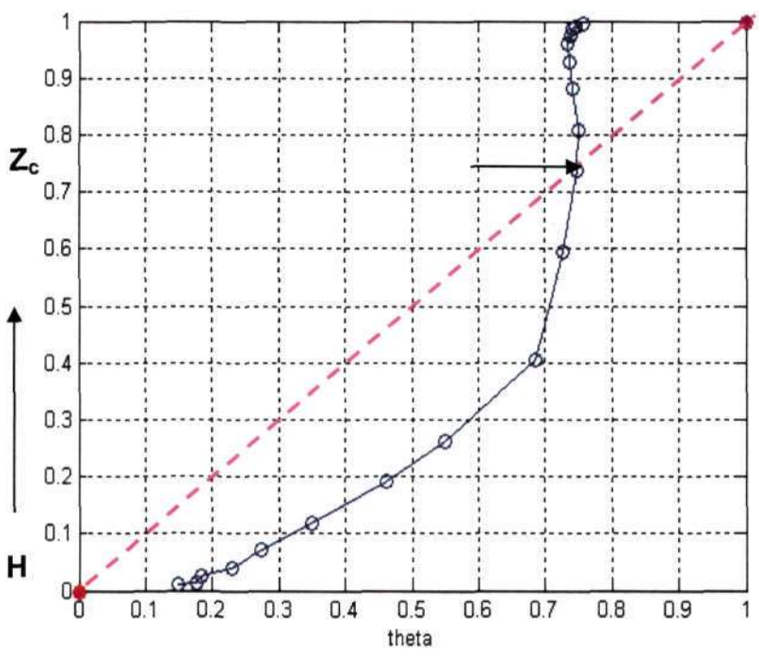

Figure 3.17. Non–dimensional Temperature profiles (Bottom: Black) [Exp. # 45]

Figure 3.18 shows the comparison of the all three cases mentioned above. Here the horizontal axis is $\delta T/\Delta T$, where δT (temperature slip) is the temperature difference of the bottom plate and thermocouple at height 1mm and ΔT is the temperature difference of the bottom plate and top of the test section. Vertical axis is non-dimensional critical height at which actual temperature profile crosses the conductive temperature profile. This figure clearly show that height of the cross over increases with decrease in the emissivity moreover temperature slip also increases with decrease in emissivity.

3.3.3 Effect of sky temperature on stable stratification

In this section we present the results for the experiments with stable stratification in the test section in which we have varied top (sky) temperature. In both of theses experiments bottom plate was of Aluminum (moderate emissivity).

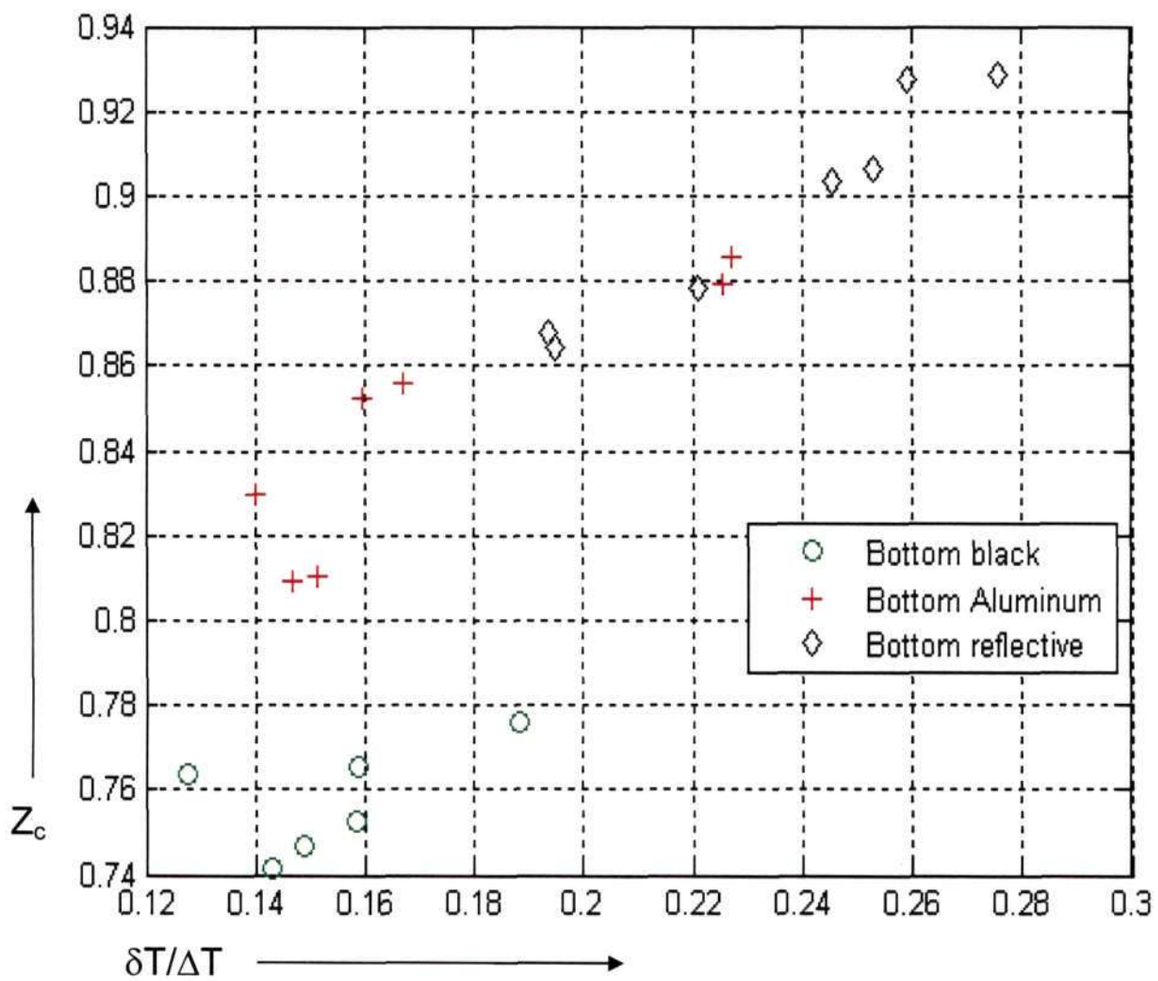

Figure 3.18. Comparison of all three cases (stable stratification)

Figure 3.19 shows the temperature profile for the case where sky (outer unit) was at a high temperature (T_{sky} =305 K). In this case result does not show much change from the results for the case where sky was at ambient temperature.

Figure 3.20 shows the time series of temperature for the experiment discussed above. All blues lines are time series inside the test section where height in the test section is increasing with the vertical axis. Red and Black lines show the time series of the bottom and top of the test section respectively while Green line shows the temperature of the sky. Time series for the case of high sky temperature is qualitatively similar to the experiments where sky was ambient temperature.

Figure 3.21 shows the temperature profile for the case where sky (outer unit) was at a low temperature (T_{sky} = 280 K). The measured temperature profile does not have a crossover point with the conductive profile as happened in the previous cases. This could be due to radiative heating of the test section but could also be due to the more than normal cooling of the top boundary of the test section. The time series corresponding to this case is shown in Figure 3.22 and is plotted in similar manner to Figure 3.20. The time series shows an interesting feature. Around 100 seconds, the sky temperature falls suddenly by about 5 degrees. Just after this episode, temperature at a height of 15, 25 and 40 mm start fluctuating more than usual. These higher than normal fluctuations are also observed at lower heights, but not to the same extent.

This phenomenon was observed on occasions, whenever the sky temperature was decreased. The reason behind this could not be understood, but appears to be of radiatively induced instability. More work is needed before any definite comments can be made.

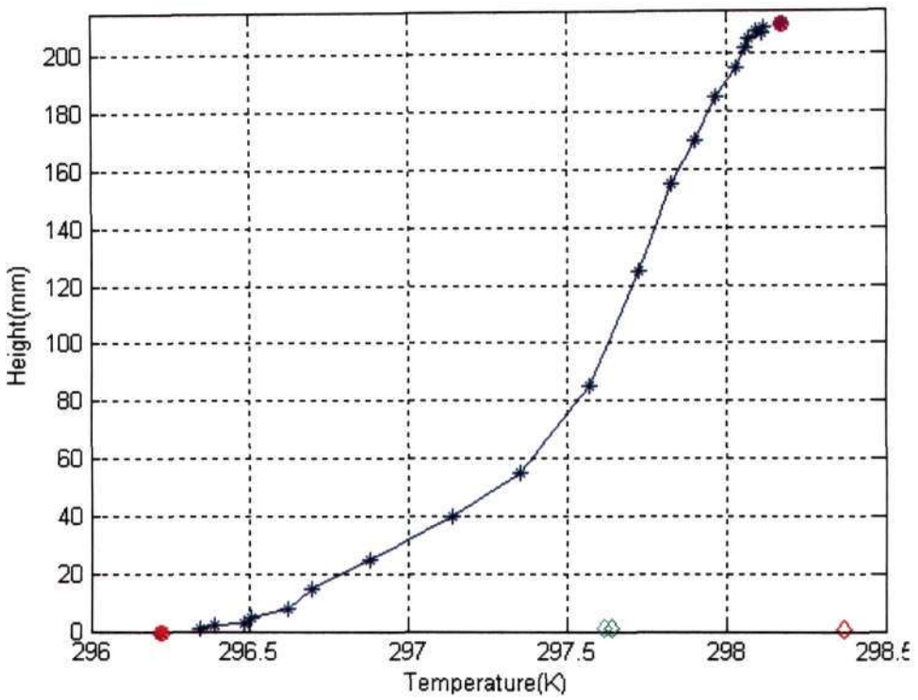

Figure 3.19. Temperature profile for high T_{sky} [Exp. # 51]

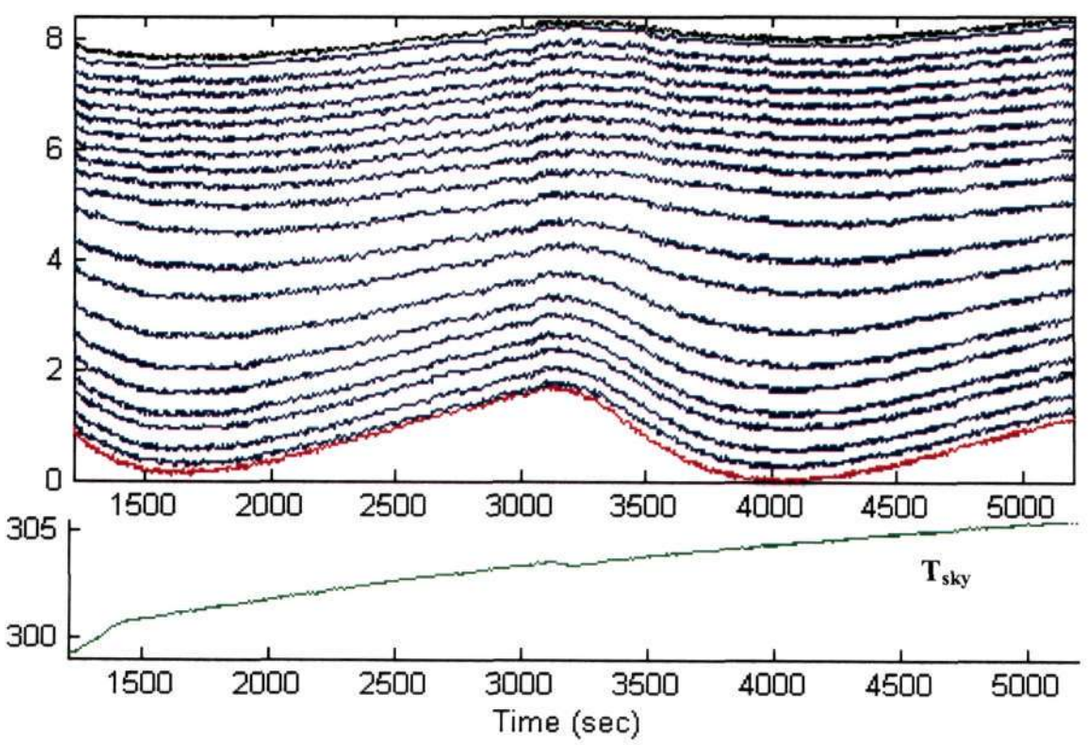

Figure 3.20. Time series for high T_{sky} [Exp. # 51]

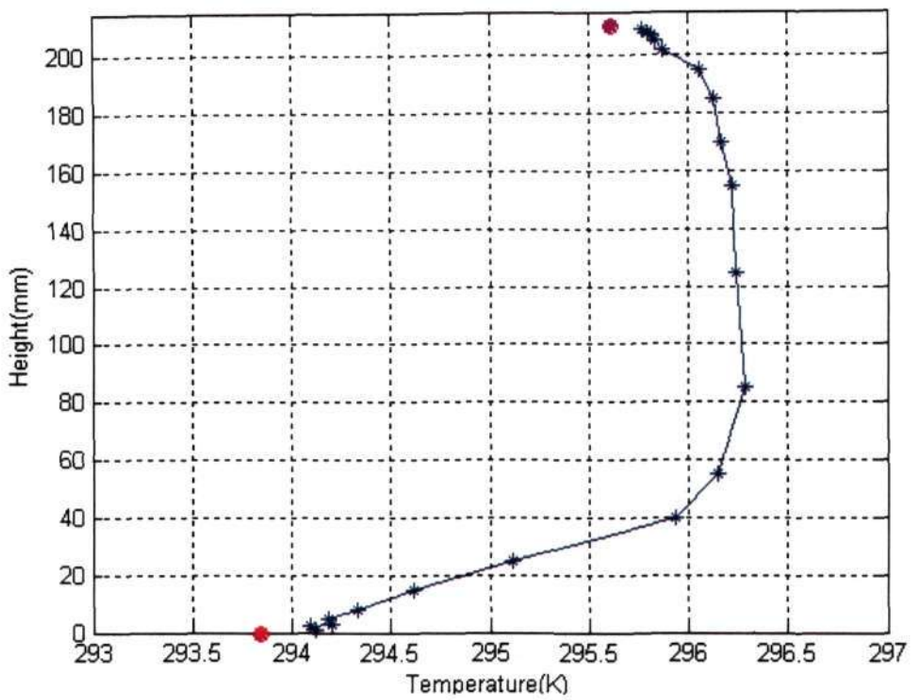

Figure 3.21. Temperature profiles for low T_{sky} [Exp. # 56]

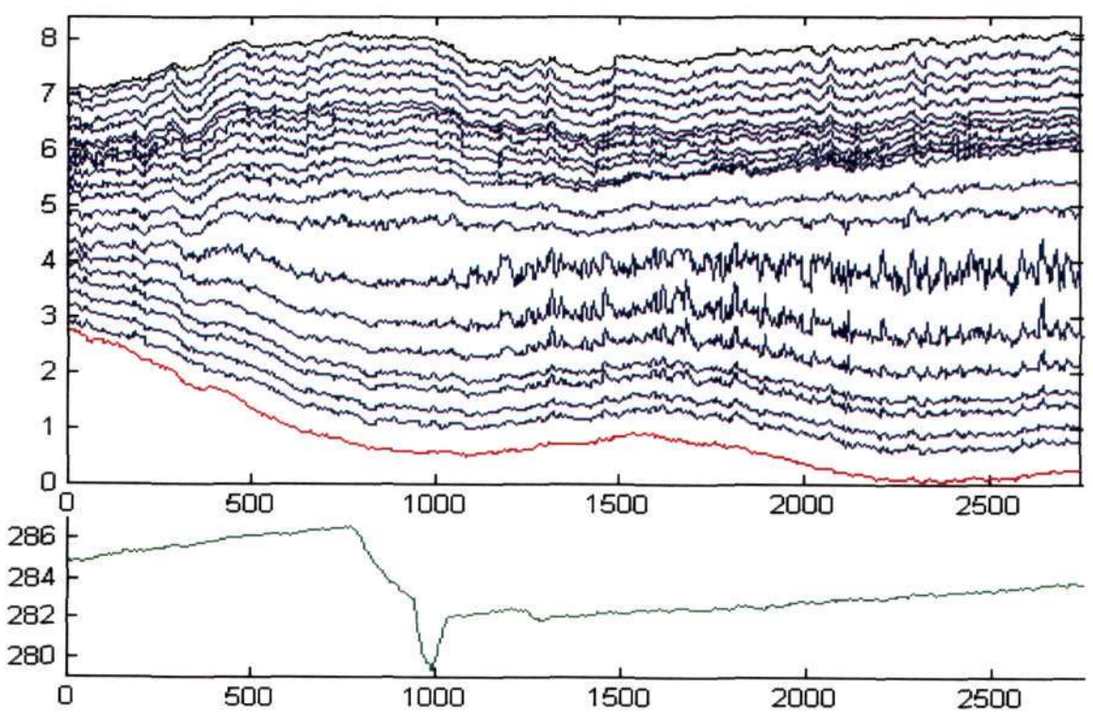

Figure 3.22. Time series for low T_{sky} [Exp. # 56]

Chapter 4 Conclusions

The thrust of the present work was to simulate the lifted temperature minimum in the laboratory conditions. Numerical simulations for the lab scale model were first carried out to determine the feasibility of reproducing the phenomenon under lab conditions and to study the effect of radiative transport on the temperature profiles in participating medium. These simulations showed that measurable intensities of the minima could indeed be obtained under conditions that were fairly easily achievable in the lab.

Taking into account the numerical simulations, a set up to obtain LTM was fabricated. The set up was made in a manner as to model the actual conditions in the field as closely as was possible. A crucial aspect of this was the decoupling of the radiative and convective boundary conditions that occurs automatically in the field. Overall, the decoupling of the radiative and convective boundary conditions shows up the effect of radiation very clearly, resulting in larger deviations from the linear conductive profile. For example compare results of Goody et.al. with present results. Figure 4.1 shows the non dimensional temperature profile for Goody's experiment. Maximum deviation from the conductive profile in his result is 2.6×10^{-2} K while in our experiments this comes of the order of 1 K.

With this setup, LTM were obtained. The intensities of these minima (around 0.5 -1.5 °C) were of the order predicted from our simulations for similar conditions but the height of the minimum from the simulation was much greater than the experiments. This could be due to the fact that the two dimensional approximation is not a good one for the set up, and as a result there could even be convective influences. There were also fluctuations in temperature observed which could be the result of natural convection.

To isolate the effect of radiation on the phenomenon, experiments were also carried out with stably stratified system.

Temperature profiles for these cases show significant deviations from the linear conductive profile, which clearly shows the effect of radiation. Again, these deviations do not agree quantitatively with those obtained from the numerical simulations, being significantly higher than those observed in the numerical simulations.

Changes in temperatures of the boundaries did not have much effect on temperature profile. However changes in ground emissivity and sky temperature did have considerable effects on the temperature profiles. The height of crossover of experimental profile from conductive profile was increased with decrease in emissivity. The temperature slip (temperature difference of the bottom plate and thermocouple at height 1mm) also increases with decrease in emissivity.

Reducing the sky temperature induced some instabilities in the temperature which require further work to understand.

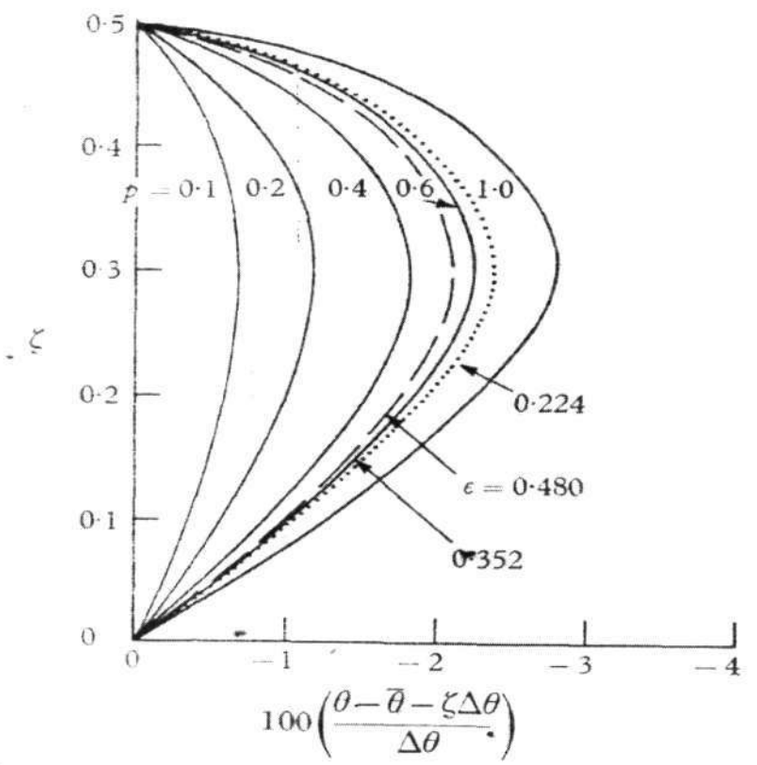

Figure 4.1. Non dimensional temperature profile from Goody's experiments [1964]

Appendix I

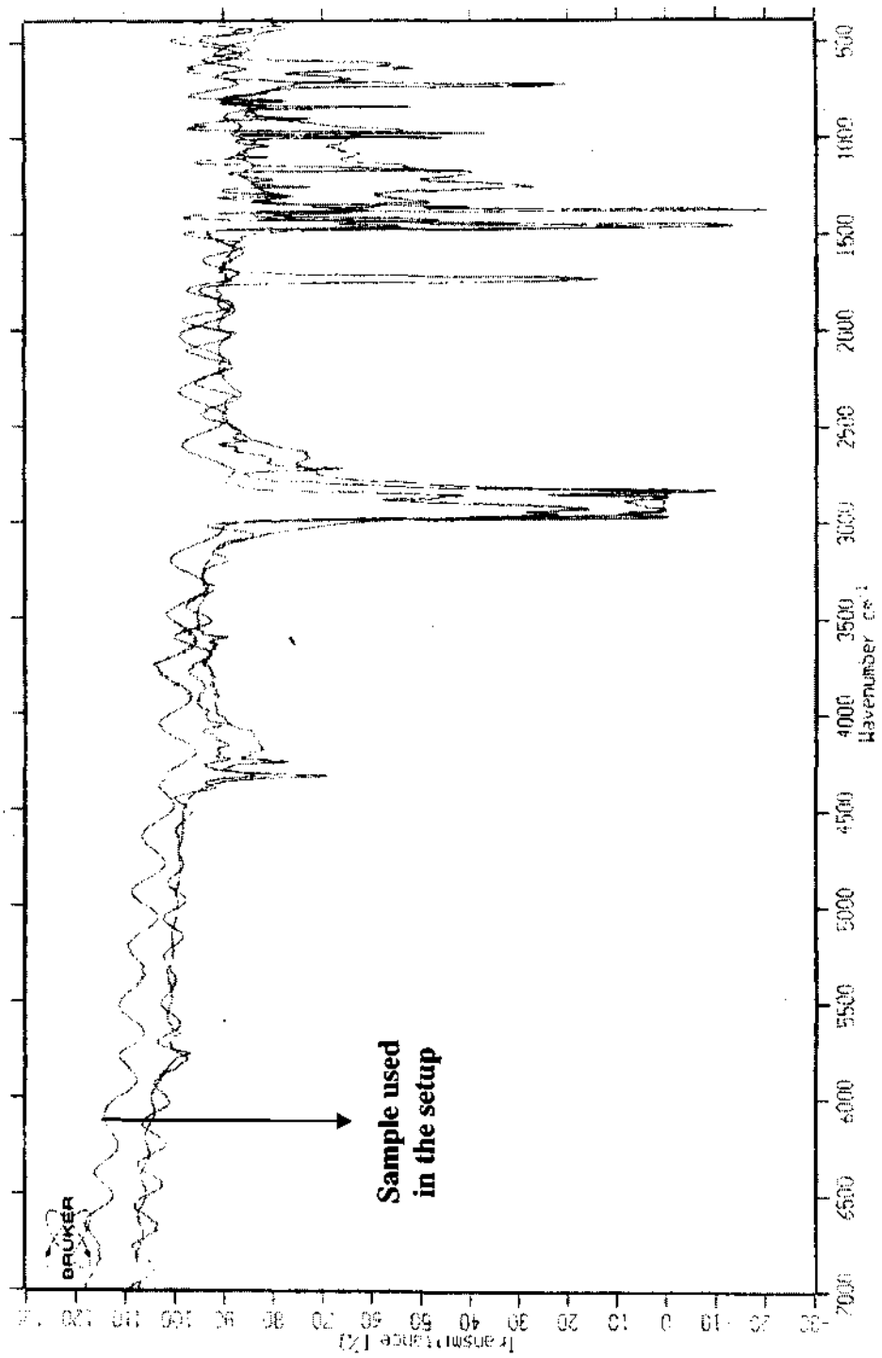

Figure.A.1. Transmissivity of different polythene samples

Appendix II: List of experiments

Experiment no.	Measurement method	Bottom surface	Density stratification
1	Traverse	Aluminum	Unstable
2	Traverse	Aluminum	Unstable
3	Traverse	Aluminum	Unstable
4	Traverse	Aluminum	Unstable
5	Traverse	Aluminum	Unstable
6	Traverse	Aluminum	Unstable
7	Traverse	Aluminum	Unstable
8	Rack(High resolution near bottom only)	Aluminum	Unstable
9	Rack(High resolution near bottom only)	Aluminum	Unstable
10	Rack(High resolution near bottom only)	Aluminum	Unstable
11	Rack(High resolution near bottom only)	Aluminum	Unstable
12	Rack(High resolution near bottom only)	Aluminum	Stable
13	Rack(High resolution near bottom only)	Aluminum	Stable
14	Rack(High resolution near bottom only)	Aluminum	Stable
15	Rack(High resolution at bottom and top)	Aluminum	Unstable
16	Rack(High resolution at bottom and top)	Aluminum	Unstable
17	Rack(High resolution at bottom and top)	Aluminum	Unstable
18	Rack(High resolution at bottom and top)	Aluminum	Unstable
19	Rack(High resolution at bottom and top)	Aluminum	Unstable
20	Rack(High resolution at bottom and top)	Aluminum	Unstable
21	Rack(High resolution at bottom and top)	Aluminum	Unstable
22	Rack(High resolution at bottom and top)	Aluminum	Unstable
23	Rack(High resolution at bottom and top)	Reflective	Stable
24	Rack(High resolution at bottom and top)	Reflective	Stable
25	Rack(High resolution at bottom and top)	Reflective	Stable
26	Rack(High resolution at bottom and top)	Reflective	Stable
27	Rack(High resolution at bottom and top)	Reflective	Stable
28	Rack(High resolution at bottom and top)	Reflective	Stable
29	Rack(High resolution at bottom and top)	Reflective	Stable
30	Rack(High resolution at bottom and top)	Reflective	Stable
31	Rack(High resolution at bottom and top)	Aluminum	Stable
32	Rack(High resolution at bottom and top)	Aluminum	Stable
33	Rack(High resolution at bottom and top)	Aluminum	Stable
34	Rack(High resolution at bottom and top)	Aluminum	Stable
35	Rack(High resolution at bottom and top)	Aluminum	Stable
36	Rack(High resolution at bottom and top)	Aluminum	Stable
37	Rack(High resolution at bottom and top)	Aluminum	Stable
38	Rack(High resolution at bottom and top)	Aluminum	Stable
39	Rack(High resolution at bottom and top)	Black	Stable
40	Rack(High resolution at bottom and top)	Black	Stable
41	Rack(High resolution at bottom and top)	Black	Stable
42	Rack(High resolution at bottom and top)	Black	Stable

43	Rack(High resolution at bottom and top)	Black	Stable
44	Rack(High resolution at bottom and top)	Black	Stable
45	Rack(High resolution at bottom and top)	Black	Stable
46	Rack(High resolution at bottom and top)	Black	Stable
47	Rack(High resolution at bottom and top)	Black	Stable
48	Rack(High resolution at bottom and top)	Black	Stable
49	Rack(High resolution at bottom and top)	Aluminum	Stable (Hot sky)
50	Rack(High resolution at bottom and top)	Aluminum	Stable (Hot sky)
51	Rack(High resolution at bottom and top)	Aluminum	Stable (Hot sky)
52	Rack(High resolution at bottom and top)	Aluminum	Stable (Hot sky)
53	Rack(High resolution at bottom and top)	Aluminum	Stable (Cold sky)
54	Rack(High resolution at bottom and top)	Aluminum	Stable (Cold sky)
55	Rack(High resolution at bottom and top)	Aluminum	Stable (Cold sky)
56	Rack(High resolution at bottom and top)	Aluminum	Stable (Cold sky)

REFERENCES

1. Coantic,M and Seguin,B.,On the interaction of turbulent and radiative transfer in the surface layer. Boundary Layer Meterology, 3, pp152-177(1971).
2. Geiger,R., The climate near the ground. Harvard Univ. Press, Cambridge, Mass.(1965)
3. Gille, J., Goody, R , Convection in a radiating gas. J.Fluid Mech, 20, pp 47-79 (1964).
4. Goody, R.M., The influence of radiative transfer on cellular convection. J.Fluid Mech, 1, pp 424-435(1956).
5. Kondratyev, K.Ya., Radiation processes in the atmosphere. Pergamon Press, New York (1972).
6. Lake, J. V., The nocturnal heat balance. Nature 176,pp 32-33(1955).
7. Lake, J. V., The temperature profile above Bare Soil on Clear Nights, Q. Jl. R. Met. Soc, 82, pp 187-197(1956 A).
8. Lake,J.V., Discussion on the paper of Lake. Q. Jl. R. Met. Soc, 82,pp 530-531(1956 B).
9. Lan, C.H., Ezekoye, O.A., Howell, J.R., Ball, K.S. Stability analysis for three-dimensional Raleigh- Benard Convection with radiatively participating medium using spectral methods. Int.J. Heat and Mass Transfer, 46, pp1371-1383 (2003).
10. Lettau, H. H., Wind and temperature profile prediction for diabatic surface layers including strong inversion cases, Boundary Layer meteorology, 17, pp 443-464(1979).
11. Liou, K.N., An introduction to atmospheric radiation. Int geophysics series., Vol. 25, Academic press (1980).
12. Moller, F, Z., Meteorol, 9, pp 47(1955).
13. Narasimha, R., When and why air can be cooler than ground just below: a theory for the Ramdas effect. J. Ind. Inst. Sci., 71, pp 471-483 (1991).
14. Narasimha, R. and Vasudeva Murthy, A. S., The energy balance in the Ramdas Layer, Boundary Layer Meteorol., 76, pp 307-321(1995).
15. Oke, T. R., The temperature profile near the ground on calm, clear nights, Q. Jl. R. Met. Soc, 96, pp 14-23(1970).
16. Paltridge,G.W. and Platt, C.M.R., Radiative processes in meteorology and climatology. Elsevier Scientific Pub Company, Amsterdam (1976).

17. Ragothaman,S., Narasimha,R., Vasudeva Murthy,A.S., The dynamical behaviour of the lifted temperature minimum. IL Nuovo Cimento, 24, pp 353-375(2001).
18. Ramdas, L. A., & Atmanathan, S., The vertical distribution of air temperature near the ground at night, Beit. Geophys. 37, pp116-117 (1932).
19. Ramanathan, K.R. and Ramdas,L.A., Derivation of Angstroms formula for atmospheric radiation and general considerations regarding nocturnal cooling of air layers near the ground. Proc.Ind.Acad.Sci., 1, pp 822-829 (1935).
20. Raschke, K., Über das nächtliche Temperaturminimum über nackten Boden in Poona, Met. Rundschau, 10, pp 1-11(1957).
21. Varghese,S., Band model computation of near-surface longwave fluxes. Phd thesis.JNCASR(2003).
22. Spiegel, E.A., The convective instability of a radiating fluid layer, Astrophys.J., 132, pp 716-728(1960).
23. Sutton, O.G., Micrometeorology: A study of physical processes in the lowest of the earth's atmosphere. McGraw-Hill Book Company Inc. (1953).
24. Vasudeva Murthy, A. S., Srinivasan, J. & Narasimha R., A Theory of the Lifted Temperature Minimum on Calm, Clear Nights, Phil. Trans. Roy. Soc. A 344, pp 183-206(1993).
25. Zdunkowski, W., The nocturnal temperature minimum above the ground, Beirt. Phys. Atmos., 59, pp 247-253(1966).
26. Zdunkowski, W. and Johnson, F.G., Infrared flux divergence calculations with newly constructed radiation tables. J. Appl. Met., 4, pp 371-377 (1965).